Molecular Pharmacology Fast Forward. Published on July 1, 2021 as DOI: 10.1124/molpharm.121.000256
This article has not been copyedited and formatted. The final version may differ from this version.

Differential Reversible and Irreversible Interactions between Benzbromarone and Human Cytochrome P450s 3A4 and 3A5

Lloyd Wei Tat Tang[1#], Ravi Kumar Verma[2#], Ren Ping Yong[1], Xin Li[3], Lili Wang[3], Qingsong Lin[3], Hao Fan[2ǂ], Eric Chun Yong Chan[1ǂ]

[1]Department of Pharmacy, Faculty of Science, National University of Singapore, Singapore

[2]Bioinformatics Institute (BII), Agency for Science, Technology and Research (A*STAR), Singapore

[3]Protein and Proteomics Centre (PPC), SingMass, National University of Singapore, Singapore

[#]*L.W.T.T and R.K.V contributed equally to the work.*

[ǂ]*H.F and E.C.Y.C are co-corresponding authors*

Molecular Pharmacology Fast Forward. Published on July 1, 2021 as DOI: 10.1124/molpharm.121.000256
This article has not been copyedited and formatted. The final version may differ from this version.

Running title:

Differential Interactions Between Benzbromarone and CYP3A4 and CYP3A5

Address correspondence to:

Professor Eric Chun Yong Chan, Department of Pharmacy, National University of Singapore, 18 Science Drive 4, Singapore 117543.

Email: phaccye@nus.edu.sg; Telephone: +65-6516 6137; Fax: +65-6779 1554

Dr Hao Fan, Bioinformatics Institute (BII), Agency for Science, Technology and Research (A*STAR), 30 Biopolis Street, Singapore 138671.

Email: fanh@bii.a-star.edu.sg; Telephone: +65-6478 8500

Number of Tables	5
Number of Figures	8
Number of References	42
Number of Words in the Abstract	235
Number of Words in the Significance Statement	80
Number of Words in the Introduction	746
Number of Words in the Discussion	1499

Molecular Pharmacology Fast Forward. Published on July 1, 2021 as DOI: 10.1124/molpharm.121.000256
This article has not been copyedited and formatted. The final version may differ from this version.

ABBREVIATIONS

BBR	Benzbromarone
CYP3A4	Cytochrome P450 3A4
CYP3A5	Cytochrome P450 3A5
DBP	Distal binding pocket
ESI	Electrospray ionization
G6P	Glucose-6-phosphate
G6PDH	Glucose-6-phosphate dehydrogenase
HPLC	High-performance liquid chromatography
IC_{50}	Half-maximal inhibitory concentration
K_B	Activator binding constant
K_m	Michaelis constant
LC/MS/MS	Liquid chromatography tandem mass spectrometry
MBI	Mechanism-based inactivation
MD	Molecular dynamics
MRM	Multiple reaction monitoring
OBS	Orthosteric binding site

Molecular Pharmacology Fast Forward. Published on July 1, 2021 as DOI: 10.1124/molpharm.121.000256
This article has not been copyedited and formatted. The final version may differ from this version.

P450	Cytochrome P450
PBP	Proximal binding pocket
PDB	Protein Data Bank
rCYP3A4	Recombinant cytochrome 3A4
rCYP3A5	Recombinant cytochrome 3A5
RMSD	Root-mean-square deviation
SASA	Solvent-accessible surface area
V_{max}	Maximum rate of reaction

Molecular Pharmacology Fast Forward. Published on July 1, 2021 as DOI: 10.1124/molpharm.121.000256
This article has not been copyedited and formatted. The final version may differ from this version.

ABSTRACT

Mounting evidence have revealed that despite the high degree of sequence homology between cytochrome P450 3A isoforms (i.e. CYP3A4 and CYP3A5), they have the propensities to exhibit vastly different irreversible and reversible interactions with a single substrate. We have previously established that benzbromarone (BBR), a potent uricosuric agent utilized in the management of gout, irreversibly inhibits CYP3A4 via mechanism-based inactivation (MBI). However, it remains unelucidated if CYP3A5 – its highly homologous counterpart – is susceptible to inactivation by BBR. Using three structurally-distinct probe substrates, we consistently demonstrated that MBI was not elicited in CYP3A5 by BBR. Our *in silico* covalent docking models and molecular dynamics simulations suggested that disparities in the susceptibilities towards MBI could be attributed to the specific effects of BBR covalent adducts on the F-F' loop. Serendipitously, we also discovered that BBR reversibly activated CYP3A5-mediated rivaroxaban hydroxylation where apparent V_{max} increased and K_m decreased with increasing BBR concentration. Fitting data to the two-site model yielded interaction factors α and β of 0.44 and 5.88, respectively, thereby confirming heterotropic activation of CYP3A5 by BBR. Furthermore, heteroactivation was suppressed by the CYP3A inhibitor ketoconazole in a concentration-dependent manner and decreased with increasing pre-incubation time, implying that activation was incited via binding of parent BBR molecule within the enzymatic active site. Finally, non-covalent docking revealed that CYP3A5 can more favorably accommodate both BBR and rivaroxaban in concert as compared to CYP3A4 which further substantiated our experimental observations.

Molecular Pharmacology Fast Forward. Published on July 1, 2021 as DOI: 10.1124/molpharm.121.000256
This article has not been copyedited and formatted. The final version may differ from this version.

Keywords: CYP3A5, CYP3A4, mechanism-based inactivation, atypical kinetics, heterotropic cooperativity, benzbromarone

Molecular Pharmacology Fast Forward. Published on July 1, 2021 as DOI: 10.1124/molpharm.121.000256
This article has not been copyedited and formatted. The final version may differ from this version.

SIGNIFICANCE STATEMENT

While we have previously demonstrated that BBR inactivates CYP3A4, it remains uninterrogated if it also elicits MBI in CYP3A5 – which shares ~85% sequence similarity with CYP3A4. Here, we report that BBR exhibits differential irreversible and reversible interactions with both CYP3A isoforms and unraveled the molecular determinants underpinning their diverging interactions. These data offer important insight into differential kinetic behavior of CYP3A4 and CYP3A5 which potentially contributes to inter-individual variabilities in drug disposition.

Molecular Pharmacology Fast Forward. Published on July 1, 2021 as DOI: 10.1124/molpharm.121.000256
This article has not been copyedited and formatted. The final version may differ from this version.

INTRODUCTION

CYP3A4 is the most abundant cytochrome P450 (P450) isoform expressed in the liver. Coupled with its wide substrate and catalytic promiscuity, it is known to be involved in the oxidative metabolism of >50% of all marketed drugs (Wilkinson, 1996; Wrighton *et al.*, 1996). Consequently, it has been the focal point of intense pharmacological research. Recently, CYP3A5 – its highly homologous counterpart – has also gained prominence in xenobiotic metabolism. While both CYP3A4 and CYP3A5 possess overlapping substrate specificities, they are known to have different relative contributions to its clearance (Tseng *et al.*, 2014). Furthermore, expression levels of CYP3A5 can vary considerably between ethnic populations due to the occurrence of the defective *3 allele that encodes for a truncated and non-functional protein. Conversely, in wild-type *1 carriers, the hepatic protein expression of CYP3A5 may be on par with, or even surpass that of CYP3A4 in some individuals (Lamba *et al.*, 2002; Lin *et al.*, 2002). As such, CYP3A5 may further augment CYP3A-mediated drug metabolism and necessitate dose adjustments (Kamdem *et al.*, 2005). Importantly, apart from their differing metabolic capacities and expression levels, mounting evidence have revealed that despite the high degree of sequence homology between both CYP3A isoforms, they have the propensities to exhibit vastly different reversible and irreversible interactions with a common substrate (Okada *et al.*, 2009; Sugiyama *et al.*, 2011; Guo *et al.*, 2019).

Mechanism-based inactivation (MBI) is one such irreversible interaction that is of clinical significance due to an irrevocable loss of enzymatic activity which can only be restored upon biosynthesis of new enzymes. Hence, the extent of pharmacokinetic drug-drug interaction (DDI) tends to be more profound than with a

Molecular Pharmacology Fast Forward. Published on July 1, 2021 as DOI: 10.1124/molpharm.121.000256
This article has not been copyedited and formatted. The final version may differ from this version.

direct reversible inhibitor (Bjornsson *et al.*, 2003). A key molecular-initiating event underscoring MBI is the prior bioactivation of the parent drug into an electrophilic reactive intermediate which subsequently primes it for covalent adduction to nucleophilic amino acid residues within the active site (Kamel and Harriman, 2013). Notably, several research groups have characterized multiple aberrant CYP3A4-mediated bioactivation pathways stemming from the benzofuran and dibrominated phenolic moiety of the uricosuric agent benzbromarone (BBR) **(Fig. 1A)** (Kitagawara *et al.*, 2015; Wang *et al.*, 2017, 2019). These findings led us to posit that BBR can potentially undergo metabolic activation to reactive electrophilic species that irreversibly inhibit CYP3A4 via MBI. Indeed, these postulations were confirmed by our recent findings which established BBR as an irreversible MBI of CYP3A4 (Tang *et al.*, 2021). However, it remains unelucidated as to whether CYP3A5 could also be susceptible to MBI by BBR. At this outset, previous studies interrogating the MBI in CYP3A4 and CYP3A5 have revealed vastly different susceptibilities and/or potencies to MBI between both isoforms (Pearson *et al.*, 2007; Hong *et al.*, 2016). Moreover, due to the comparatively larger active site in CYP3A isoforms, probe substrate-specific inactivation has also been observed (Chan *et al.*, 2012). Taken together, it is therefore imperative to interrogate the MBI susceptibilities of both CYP3A isoforms to BBR individually using an array of structurally-distinct probe substrates to investigate if it elicits any isoform- or probe substrate-specific inactivation.

Moreover, CYP3A isoforms may also be implicated in reversible atypical kinetic interactions. Atypical P450 kinetics deviate from the conventional Michaelis-Menten model due to non-fulfillment of assumptions crucial to the derivation of its kinetic parameters hence confounding estimation of *in vitro* intrinsic clearances which

Molecular Pharmacology Fast Forward. Published on July 1, 2021 as DOI: 10.1124/molpharm.121.000256
This article has not been copyedited and formatted. The final version may differ from this version.

hinders accurate *in vitro-in vivo* extrapolations. Examples of such atypical kinetic phenomena include substrate inhibition and homotropic/heterotropic cooperativity among many others (Tracy, 2006). While atypical kinetics are uncommon, they are more frequently reported with CYP3A isoforms. Although the exact mechanistic basis underpinning such observation remains nebulous, it is thought to be ascribed to the presence of a highly plastic active site that is capable of accommodating multiple substrates simultaneously with different binding modes (Sevrioukova and Poulos, 2013). In that regard, the crystal structure of CYP3A5 has been recently solved (Hsu *et al.*, 2018; Hsu and Johnson, 2019). Remarkably, analysis of its active site topology revealed salient plasticity differences between CYP3A4 and CYP3A5. To date, it remains unknown if the CYP3A isoforms exhibit atypical kinetics with BBR. As such, assessment of potential atypical kinetics needs to be discerned between CYP3A4 and CYP3A5

In this study, we investigated the specific nature of interactions between BBR and the CYP3A isoforms. Our *in vitro* results revealed that BBR irreversibly inhibits CYP3A4 via MBI whereas it reversibly activates CYP3A5-mediated rivaroxaban hydroxylation through heterotropic cooperative interactions. Our *in silico* findings further provided plausible mechanistic insights on the structural and molecular determinants underpinning their diverging interaction profiles.

Molecular Pharmacology Fast Forward. Published on July 1, 2021 as DOI: 10.1124/molpharm.121.000256
This article has not been copyedited and formatted. The final version may differ from this version.

MATERIALS AND METHODS

Chemicals and Reagents. BBR and testosterone were obtained from Tokyo Chemical Industries (Tokyo, Japan). Dexamethasone, ketoconazole, prednisolone and carbamazepine were acquired from Sigma-Aldrich (St. Louis, MO). Rivaroxaban was purchased from Carbosynth (Berkshire, UK). Midazolam was procured from Tocris Bioscience (Bristol, UK). Human recombinant cytochrome P450 3A4 and 3A5 Supersomes (1000 pmol/mL) (rCYP) co-expressing cytochrome b_5 and NADPH-P450 reductase and the NADPH regenerating system comprising NADP+ and glucose-6-phosphate (G6P) (NADPH A) and glucose-6-phosphate dehydrogenase (G6PDH) (NADPH B) were purchased from BD Gentest (Woburn, MA). HPLC-grade acetonitrile was acquired from Tedia Company Inc. (Fairfield, OH). Ultrapure water (type I) was obtained using a Milli-Q water purification system (Millipore Corporation, Bedford, MA). All other commercially available chemicals were of analytical or HPLC-grade.

Screening of MBI of CYP3A4 and CYP3A5 by BBR. The potential MBI of CYP3A4 and CYP3A5 by BBR was first evaluated by preparing primary incubation mixtures (n = 3) consisting of 20 pmol/mL rCYP3A4 or rCYP3A5, BBR (at either 0, 5 or 25 µM – with the latter two corresponding to low and high concentrations respectively), G6PDH and 100 mM potassium phosphate buffer (pH 7.4). The enzymatic reaction was initiated via the addition of NADP+/G6P after pre-warming at 37°C for 5 min. The final primary incubation mixture (100 µL) contained <1% v/v organic solvent. At various pre-incubation intervals (0, 3, 8, 15, 22 and 30 min), a 5 µL aliquot of each primary incubation mixture was withdrawn and transferred to 95 µL of pre-warmed secondary incubation mixture consisting of a CYP3A-specific probe substrate, an

Molecular Pharmacology Fast Forward. Published on July 1, 2021 as DOI: 10.1124/molpharm.121.000256
This article has not been copyedited and formatted. The final version may differ from this version.

NADPH regenerating system and 100 mM potassium phosphate buffer (pH 7.4). This yielded a 20-fold dilution. Specifically, three structurally-disparate substrates of CYP3A at concentrations more than ~4× their respective K_m were included in our screening assay (i.e. 200 µM testosterone, 25 µM midazolam and 50 µM rivaroxaban). The secondary incubation mixtures were incubated at 37°C for an additional 10 min (for assays involving testosterone or midazolam) or 2 h (for experiments involving rivaroxaban). After which, an 80 µL aliquot was immediately removed and quenched with equal volumes of ice-cold acetonitrile spiked with either 1 µM prednisolone (internal standard for quantification of 6β-hydroxytestosterone and 1'-hydroxymidazolam) or 4 µM dexamethasone (internal standard for quantification of hydroxylated rivaroxaban). The quenched samples were centrifuged at 4000*g* at 4°C for 30 min to obtain the supernatant for LC/MS/MS analysis.

Substrate Depletion of BBR in CYP3A4 and CYP3A5. Incubation mixtures comprising 20 pmol/mL rCYP3A4 or rCYP3A5, 1 µM BBR, G6PDH and 100 mM potassium phosphate buffer (pH 7.4) were prepared in triplicates. After pre-incubating at 37°C for 5 min, the reaction was initiated via the addition of NADP+/G6P. The final primary incubation mixture (100 µL) contained <1% v/v organic solvent. Subsequently, at various intervals (0, 5, 10, 15, 30, 60 and 120 min), an 80 µL aliquot of each incubation mixture was withdrawn and quenched with equal volumes of ice-cold acetonitrile spiked with 10 nM carbamazepine (internal standard). The quenched samples were then centrifuged at 4000*g* at 4°C for 30 min, following which aliquots of the supernatant was sampled to quantify the amount of BBR remaining using LC/MS/MS.

Molecular Pharmacology Fast Forward. Published on July 1, 2021 as DOI: 10.1124/molpharm.121.000256
This article has not been copyedited and formatted. The final version may differ from this version.

CYP3A5 Molecular Dynamics (MD) Simulations. The apo- (PDB:6MJM) and holo- (PDB:5VEU) CYP3A5 crystal structures were first downloaded from RCSB Protein Data Bank (PDB) and processed using the protein preparation wizard in Maestro (Schrödinger, New York) (Rose *et al.*, 2015). Briefly, for each protein structure retrieved, only chain A was considered. All heteroatoms except for the protein, heme prosthetic group and co-crystallized ligand (if available) were removed from the structure. Thereafter, the missing residues and side chains were added using Prime (Schrödinger, New York) and the ionization states of titratable groups were determined using Epik (Schrödinger, New York). Following which, the simulation systems for each of the conditions (apo and holo) were built using CHARMM-GUI (Jo *et al.*, 2008). In the holo condition, the GROMACS compatible parameters for ritonavir (bound ligand for PDB:5VEU) were generated using Antechamber (Wang *et al.*, 2006). The physiological concentration of 150 mM NaCl was maintained by adding an appropriate amount of Na^+ and Cl^- ions. In total, each solvated system consisted of approximately 100,000 atoms. MD simulations were carried out using GROMACS 2018.2 (Abraham *et al.*, 2015) with the CHARMM36 forcefield for proteins (Best *et al.*, 2012) and the CHARMM TIP3P water model (Jorgensen *et al.*, 1983). Energy minimization and equilibration of the system were conducted using standard CHARMM-GUI steps. Briefly, the system was first minimized using the steepest descent following a 125 ps equilibration step. During the equilibration, positional restrains of 400 and 40 kJ/mol/nm^2 were imposed on the protein backbone and side-chain heavy atoms, respectively. To improve sampling, we generated 20 equilibration trajectories with different random number seeds in replicates. Following which, each equilibrated system was subjected to a production run of 20 ns without

Molecular Pharmacology Fast Forward. Published on July 1, 2021 as DOI: 10.1124/molpharm.121.000256
This article has not been copyedited and formatted. The final version may differ from this version.

any positional restraint. All production runs were performed in a constant particle, pressure and temperature (NPT) ensemble. Specifically, the temperature was kept at a constant 310 K using Nosé-Hoover thermostat (Hoover, 1985) whereas the pressure of 1 bar was maintained using Parrinello-Rahman pressure coupling (Nosé and Klein, 1983). Long-range interactions were calculated using the particle-mesh Ewald (PME) method (Darden *et al.*, 1993) and van der Waals' interactions were described using a cut-off of 12 Å for all simulations. Periodic boundary conditions (PBC) were employed in all three directions. As CYP3A4 and CYP3A5 sequence alignment revealed considerable differences in the F-F' loop and C-terminal region of these proteins. We created an *in silico* apo-CYP3A5 double mutant (G214D/Q479G) ($CYP3A5_{MUT}$) in which Gly214 and Gln479 on the F-F' loop was replaced by Asp and Gly as observed in CYP3A4 to ascertain the biochemical implications of these variations. An additional set of 20 trajectories (20 ns each) were collected for the apo-$CYP3A5_{MUT}$. In total, we collected 1.2 μs long trajectory data for all three conditions (apo-$CYP3A5_{WT}$, holo-$CYP3A5_{WT}$, apo-$CYP3A5_{MUT}$)

Root-Mean-Square Deviation (RMSD)-based Hierarchical Clustering. RMSD-based clustering was performed on apo- and holo-CYP3A5 trajectories. Briefly, we first concatenated all apo- and holo-CYP3A5 trajectories and computed the pairwise RMSD matrix. In particular, the heavy atoms of the heme prosthetic group were utilized for superimposition and the pairwise RMSD was calculated for residues 209-243 and 465-490 which comprises the F-F' loop (residue 211-220) and C-terminal loop. The computed RMSD matrix was then subjected to clustering using the hierarchical-clustering algorithm implemented in SciPy with an RMSD cut-off of 3 Å.

Molecular Pharmacology Fast Forward. Published on July 1, 2021 as DOI: 10.1124/molpharm.121.000256
This article has not been copyedited and formatted. The final version may differ from this version.

Finally, MD frames representing the centroid of the clusters were extracted for subsequent covalent docking.

***In silico* Ligand Preparation.** Ligands for the covalent docking were prepared as previously described (Tang *et al.*, 2021). Briefly, we obtained 3D coordinates of BBR from the PubChem Database (Kim *et al.*, 2018), from which two epoxide metabolites, namely, benzbromarone-6,7-benzofuran-epoxide (BBR-6,7-BF-Epoxide) **(Fig. 1B)** and benzbromarone-5,6-benzofuran-epoxide (BBR-5,6-BF-Epoxide) **(Fig. 1C)** were derived using the sketcher module in the Schrödinger suite (Schrödinger, New York). Thereafter, the lowest energy conformer was generated for both epoxide metabolites using the LigPrep (Schrödinger, New York).

***In silico* Binding Site Prediction and Covalent Docking.** Covalent docking was performed as previously described (Tang *et al.*, 2021). Briefly, potential ligand-binding pockets for each of the included MD frames and CYP3A5 crystal structures were first identified using the site recognition software Sitemap (Schrödinger, New York). As our previous work suggested that BBR epoxides could covalently alkylate cysteine residues vicinal to the F-F' loop and adversely modulate its flexibility, we first directed our focus to the cysteine residues in CYP3A5 that are in close proximity to the F-F' loop. Interestingly, unlike CYP3A4, there was an absence of cysteine residues near the F-F' loop of CYP3A5. Consequently, we computed a list of accessible serine residues in binding pockets that lie near the F-F' loop using an *in-house* analytical algorithm. The docking of BBR-6,7-BF-Epoxide and BBR-5,6-BF-Epoxide was performed in two sequential stages. We first non-covalently docked the metabolites in the binding pockets containing the accessible serine using GLIDE (Friesner *et al.*, 2004). If non-covalent docking was successful, we then performed

Molecular Pharmacology Fast Forward. Published on July 1, 2021 as DOI: 10.1124/molpharm.121.000256
This article has not been copyedited and formatted. The final version may differ from this version.

covalent docking for accessible serine residue within the pocket using CovDock (Zhu *et al.*, 2014) in the Schrödinger suite. In particular, we docked each BBR epoxide metabolite to Ser206 and Ser239. The covalent docking scores obtained were then combined, sorted and ranked.

Mixed-type Inhibition of CYP3A4 and CYP3A5 by BBR. The mixed-type inhibition of BBR against CYP3A4 and CYP3A5 was investigated using three structurally-distinct probe substrates (i.e. testosterone, midazolam and rivaroxaban). All experiments were conducted in triplicates in 96-well plates. Reaction mixtures for IC_{50} experiments consisted of either 20 pmol/mL rCYP3A4 or rCYP3A5, BBR (0, 0.1, 0.3, 1, 3, 10, 30 and 100 µM), probe substrate (50 µM testosterone, 3 µM midazolam or 10 µM rivaroxaban), G6PDH and 100 mM potassium phosphate buffer (pH 7.4). After pre-warming at 37°C for 5 min, the reaction was initiated via the addition of NADP+/G6P, yielding a final primary incubation mixture (100 µL) with <1% v/v organic solvent. The reaction mixture was incubated at 37°C for 10 min (for assays involving testosterone or midazolam) or 2 h (for experiments involving rivaroxaban). Following which, aliquots of the samples were quenched, centrifuged and subjected to LC/MS/MS analysis for the quantitation of either 6β-hydroxytestosterone, 1'-hydroxymidazolam or hydroxylated rivaroxaban.

Calculation of Mixed-type Inhibition Parameters (IC_{50}). The IC_{50} value was determined using the log(inhibitor) vs. normalized response – variable slope model based on **Equation 1** in GraphPad 8.0.2 (San Diego, CA)

$$Y = \frac{100}{(1 + 10^{(logIC50 - [I]) \times Hil\ slope})} \quad (1)$$

Molecular Pharmacology Fast Forward. Published on July 1, 2021 as DOI: 10.1124/molpharm.121.000256
This article has not been copyedited and formatted. The final version may differ from this version.

where IC_{50} represents the half-maximal inhibitory concentration, [*I*] is the *in vitro* concentration of the mixed-type inhibitor, Hill slope is the Hill coefficient and Y is the % enzyme activity compared to control.

Heterotropic Activation of CYP3A5-mediated Rivaroxaban Hydroxylation by BBR. The heteroactivation kinetics of CYP3A5-mediated rivaroxaban hydroxylation was investigated under time-linear conditions (i.e. 2 h) (data not shown) in 96-well plates by preparing incubation mixtures containing 20 pmol/mL rCYP3A5, BBR (0, 1, 3 and 10 µM), rivaroxaban (2.5, 5, 15, 30 and 50 µM), G6PDH and 100 mM potassium phosphate buffer (pH 7.4) in triplicates. After pre-incubating at 37°C for 5 min, the reaction was initiated via the addition of NADP+/G6P and further incubated at 37°C for 2 h. The final primary incubation mixture (100 µL) contained <1% v/v organic solvent. Subsequently, aliquots of the samples were quenched, centrifuged and subjected to LC/MS/MS analysis for the quantitation of hydroxylated rivaroxaban.

Calculation of Heteroactivation Kinetic Parameters. Kinetic constants (i.e. V_{max} and K_m) were derived from nonlinear least-square regression analysis by fitting hydroxylated rivaroxaban formation data collected at various rivaroxaban and BBR concentration to the Michaelis-Menten equation **(Equation 2)** in GraphPad 8.0.2 (San Diego, CA).

$$v = \frac{V_{\max} \times [S]}{K_m + [S]} \qquad (2)$$

Molecular Pharmacology Fast Forward. Published on July 1, 2021 as DOI: 10.1124/molpharm.121.000256
This article has not been copyedited and formatted. The final version may differ from this version.

where v is the rate of enzyme activity, V_{max} (maximum rate of reaction) and K_m (Michaelis constant) are kinetic constants for substrate metabolism; [*S*] is the *in vitro* concentration of substrate.

Additionally, the data was also fitted to nonlinear least-square regression based on the two-site model equation **(Equation 3)** (Korzekwa *et al.*, 1998) using Sigma Plot 14.0 (San Jose, CA) for three-dimensional surface plot analysis of rivaroxaban hydroxylation in the presence of BBR.

$$v = \frac{V_{\max} \times [S]}{K_{\mathrm{m}} \dfrac{\left(1 + \dfrac{[B]}{K_{\mathrm{B}}}\right)}{\left(1 + \dfrac{\beta[B]}{\alpha K_{\mathrm{B}}}\right)} + [S] \dfrac{\left(1 + \dfrac{[B]}{\alpha K_{\mathrm{B}}}\right)}{\left(1 + \dfrac{\beta[B]}{\alpha K_{\mathrm{B}}}\right)}} \qquad (3)$$

where V_{max} (maximum rate of reaction) and K_m (Michaelis constant) are kinetic constants for substrate metabolism, [*S*] is the *in vitro* substrate concentration, [*B*] is the *in vitro* activator concentration, K_B is the activator binding constant and, α and β are interaction factors indicating changes in K_m and V_{max} resulting from activator binding, respectively. In which, α and β < 1 is indicative of a decrease in K_m or V_{max}, respectively, whereas α and β > 1 represents an increase in K_m or V_{max}, respectively. For activation, α < 1 and/or β > 1. **Equation 3** only takes into consideration metabolism of the probe substrate (i.e. rivaroxaban) and assumes that product release is fast relative to oxidation rates, rapid equilibrium and single occupancy – in that only a single molecule of the probe substrate (i.e. rivaroxaban) and activator (i.e. BBR) are bound to the enzymatic active site simultaneously.

Effect of CYP3A Inhibitor on Heteroactivation. To investigate if heteroactivation of CYP3A5-mediated rivaroxaban hydroxylation can be abolished by CYP3A5

Molecular Pharmacology Fast Forward. Published on July 1, 2021 as DOI: 10.1124/molpharm.121.000256
This article has not been copyedited and formatted. The final version may differ from this version.

inhibition, the potent CYP3A competitive inhibitor ketoconazole, at a concentration of 0.1 and 1 μM (roughly 1× and 10× the K_i for CYP3A5 (Greenblatt *et al.*, 2011)), was introduced in triplicates to the primary incubation mixture comprising 20 pmol/mL CYP3A5, BBR (0, 0.1, 0.3, 1, 3, 10 and 30 μM), rivaroxaban (10 μM), G6PDH and 100 mM potassium phosphate buffer (pH 7.4). The reaction was initiated by the addition of NADP+/G6P after pre-incubation at 37°C for 5 min. Following incubation at 37°C for 2 h, aliquots of the samples were quenched, centrifuged and subjected to LC/MS/MS analysis for the quantitation of hydroxylated rivaroxaban. Incubation mixtures that excluded the addition of either ketoconazole or both BBR and ketoconazole served as the negative controls.

Effect of Pre-Incubation on Heteroactivation. Incubation mixtures consisting of 20 pmol/mL CYP3A5, BBR (0 or 10 μM), G6PDH and 100 mM potassium phosphate buffer (pH 7.4) were prepared in triplicates. After pre-warming at 37°C for 5 min, the reaction was initiated via the introduction of NADP+/G6P, yielding a final primary incubation mixture (99 μL) with <1% v/v organic solvent. At various time points (0, 10 and 20 min), 10 μM rivaroxaban (1 μL) was added into the incubation mixture and the reaction was allowed to continue for another 2 h at 37°C. Following which, aliquots of the samples were quenched, centrifuged and subjected to LC/MS/MS analysis for the quantitation of hydroxylated rivaroxaban.

Non-Covalent Docking of BBR and Rivaroxaban in CYP3A4 and CYP3A5. To elucidate possible structural insights underpinning the differential susceptibilities of both CYP3A isoforms to heteroactivation by BBR, we independently docked BBR and rivaroxaban to CYP3A4 and CYP3A5. Briefly, we first arbitrarily divided the CYP3A orthosteric binding site (OBS) into two separate cavities – namely the

Molecular Pharmacology Fast Forward. Published on July 1, 2021 as DOI: 10.1124/molpharm.121.000256
This article has not been copyedited and formatted. The final version may differ from this version.

proximal binding pocket (PBP), which is the spatial region of the OBS located within 15 Å from the heme iron, and the distal binding pocket (DBP) which comprises the rest of the binding pocket not subsumed under the PBP. A second series of RMSD-based hierarchical clustering was conducted on CYP3A4 and CYP3A5 crystal structures and/or MD frames using OBS residues which yielded a total of 4 crystal structures from CYP3A4 and 1 crystal structure along with 3 MD frames from CYP3A5 for non-covalent docking. Here, we employed two docking schemes which consisted of two individual non-covalent docking stages. In the first docking scheme, we first non-covalently docked BBR to the PBP and generated 100 docking poses. A top-scoring ligand docking pose where the hydroxyl oxygen atom in the 2,6-dibromophenol group of BBR oriented within 5 Å of the heme iron was selected and utilized to perform a second round of docking in which rivaroxaban was docked in the DBP. Conversely, in the second docking scheme, we first docked rivaroxaban to the PBP followed by BBR to the DBP. As per the previous scheme, we also generated 100 docking poses for rivaroxaban in the PBP which yielded a top-scoring ligand docking pose where the oxygen atom in the morpholinone moiety of rivaroxaban oriented within 5 Å of the heme iron was selected for a second round of docking. To evaluate and compare the extent of binding of BBR and rivaroxaban in the OBS of CYP3A4 and CYP3A5, we computed the overall OBS volume and solvent-accessible surface area (SASA) of the ligand bound in the DBP. SASA values obtained were then further converted into percentage ligand exposure using **Equation 4**

$$Ligand\ exposure\ (\%) = \frac{\mathrm{SASA_{bound}}}{\mathrm{SASA_{free}}} \times 100 \qquad (4)$$

Molecular Pharmacology Fast Forward. Published on July 1, 2021 as DOI: 10.1124/molpharm.121.000256
This article has not been copyedited and formatted. The final version may differ from this version.

where $SASA_{bound}$ and $SASA_{free}$ represent the SASA of the ligand in bound and free form respectively. Higher SASA and ligand exposure values are indicative of weaker protein-ligand interactions.

Measurement of Residual CYP3A Activity and BBR via LC/MS/MS. All samples were analyzed using the liquid chromatography tandem mass spectrometry (LC/MS/MS) system consisting of an Agilent 1290 Infinity ultra-high pressure liquid chromatography (Agilent Technologies Inc., Santa Clara, CA) interfaced with AB SCIEX Triple Quad 3500 tandem mass spectrometry system (AB SCIEX, Framingham, MA). Chromatographic separation was achieved with an ACQUITY UPLC BEH C_{18}, 1.7 µm, 2.1 × 50 mm column (Waters, Milford, MA). The aqueous mobile phase (A) was 0.1% formic acid in water, whereas the organic mobile phase (B) was 0.1% formic acid in acetonitrile. Mobile phases were delivered at a flow rate of 0.5 mL/min. The column and sample temperature were set at 45°C and 4°C respectively. The gradient elution conditions were as follows: linear gradient from 20 to 80% B (0 – 1.20 min), isocratic at 100% B (1.21 – 2.00 min) and isocratic at 20% B (2.01 – 2.50 min). All analytes were detected in positive electrospray ionization (ESI) mode. The source-dependent MS parameters are as follows: ion spray voltage = 5500 V; source temperature = 500°C; curtain gas (CUR) = 25 psi; ion source gas 1 (sheath gas) = 30 psi; ion source gas 2 (drying gas) = 30 psi. The MRM transitions and compound-dependent MS parameters of the analytes are summarized in **Supplementary Table 1**. Chromatographic peak integration was performed using SCIEX OS version 1.5.0.23389 (AB SCIEX, Framingham, MA). For all LC/MS/MS analyses, the peak area of the analyte was expressed as a ratio to the peak area of the internal standard.

Molecular Pharmacology Fast Forward. Published on July 1, 2021 as DOI: 10.1124/molpharm.121.000256
This article has not been copyedited and formatted. The final version may differ from this version.

RESULTS

Absence of Time-Dependent Inactivation of CYP3A5 by BBR. Our screening experiments revealed that BBR elicited a time- and concentration-dependent reduction in CYP3A4 activity in all three probe substrates utilized **(Fig. 2A – C)** which corroborates our previous findings on the irreversible covalent MBI of CYP3A4 by BBR (Tang *et al.*, 2021). Additionally, covalent modification of the CYP3A4 apoprotein and/or destruction of the prosthetic heme (i.e. via alkylation or oxidative fragmentation) by BBR is further substantiated by our ESI-LC/MS analyses which demonstrated that the intensity of the native CYP3A4 spectrum peak decreased by approximately 30.3% when coincubated with 50 μM BBR for 30 min as compared to vehicle controls (refer to **Supplementary Materials; Supplementary Fig. 1A – D** for more details). In contrast, time-dependent reduction in CYP3A5 activity by BBR was not observed in all three probe substrates utilized **(Fig. 2D – F)**. As MBI hinges on the prior bioactivation of the substrate to a reactive intermediate, we performed substrate depletion studies to ascertain if BBR are substrates of CYP3A4 and CYP3A5. Measuring the amount of parent drug remaining over 2 h revealed that both CYP3A isoforms were capable of metabolizing BBR, but with different efficiencies. Specifically, the percentage of BBR remaining after 2 h (expressed as mean ± S.D) was 52.62 ± 1.82 % in CYP3A4 incubations and 81.51 ± 0.29 % in CYP3A5 incubations **(Supplementary Fig. 2)**. These results confirm that BBR is a substrate of both CYP3A isoforms – with BBR being metabolized to a lower extent by CYP3A5.

CYP3A5 Crystal Structure Analysis. To gain mechanistic insights on the structural determinants underpinning the differential MBI susceptibilities to BBR in CYP3A4

Molecular Pharmacology Fast Forward. Published on July 1, 2021 as DOI: 10.1124/molpharm.121.000256
This article has not been copyedited and formatted. The final version may differ from this version.

and CYP3A5, we closely compared the crystal structures of both these CYP3A isoforms. Notably, there was an absence of cysteine residues near the F-F' loop of CYP3A5. Rather, the two cysteine residues (i.e. Cys58 and Cys239) that we previously determined to lie close to the F-F' loop in CYP3A4 were substituted to Trp58 and Ser239 in CYP3A5 **(Supplementary Fig. 3)**. Consequently, we directed our search towards nucleophilic serine residues in CYP3A5. Our structural analysis identified two accessible serine residues, namely Ser206 and Ser239, near the F-F' loop in CYP3A5 that were predicted to be amenable to covalent binding by BBR epoxide metabolites.

CYP3A5 MD Simulations. Due to the availability of only two reported crystal structures (i.e. PDB: 6MJM and 5VEU) (Hsu *et al.*, 2018; Hsu and Johnson, 2019), multiple short MD simulations were performed for holo- and apo-CYP3A5 to generate an ensemble of CYP3A5-associated MD frames. This allows for a meaningful comparison of covalent docking results to be made with CYP3A4 which possesses multiple holo and apo crystal structures. Here, our simulations yielded a total of 40 MD trajectories (20 for each condition) with a cumulative length of 800 ns (400 ns for each condition). Subsequently, after concatenating and superimposing all trajectories, RMSD-based clustering segregated frames into 28 distinct clusters. MD frames representing the centroid of each cluster were extracted for subsequent covalent docking.

CYP3A5 Covalent Docking. BBR-6,7-BF-Epoxide and BBR-5,6-BF-Epoxide were covalently docked to 28 representative frames obtained from our MD trajectory clustering analysis along with the previously reported apo (PDB:6MJM) and holo (ritonavir-bound) (PDB:5VEU) CYP3A5 crystal structures. Results from our covalent

Molecular Pharmacology Fast Forward. Published on July 1, 2021 as DOI: 10.1124/molpharm.121.000256
This article has not been copyedited and formatted. The final version may differ from this version.

docking demonstrated that BBR-adducts at Ser239 could similarly adopt a binding pose adjacent to (minimum distance <3.5 Å) the F-F' loop **(Fig. 3) (Supplementary Table 2)**. Moreover, the top covalent docking scores obtained for BBR-6,7-BF-Epoxide and BBR-5,6-BF-Epoxide adducts in CYP3A5 (-4.4, -3) **(Table 1)** were comparable to scores previously reported for CYP3A4 (-3.1, -3.5) **(Table 1)** (Tang *et al.*, 2021). Taken together, our findings suggest that both CYP3A4 and CYP3A5 have similar propensities to form adducts with BBR epoxide metabolites.

Our previous covalent docking models with CYP3A4 demonstrated that BBR-Cys239 adducts could stabilize a single F-F' loop conformation in which the F-F' loop residues are positioned in close proximity to the C-terminal loop (termed as the 'closed' conformation) **(Fig. 4C)**. Interestingly, this 'closed' conformation was also observed in apo (PDB:1TQN) and holo (ritonavir-bound) (PDB:3NXU) crystal structures of CYP3A4 **(Fig. 4A and B)** (Yano *et al.*, 2004; Sevrioukova and Poulos, 2010). Comparative analysis of covalent docking poses in CYP3A5 revealed that BBR-Ser239 adducts could stabilize two structurally-distinct F-F' loop conformations. On one hand – as evident in cluster-13, the resulting stabilized F-F' loop may adopt the 'closed' conformation that is also seen in the apo (PDB:6MJM) and holo (ritonavir-bound) (PDB:5VEU) CYP3A5 crystal structures **(Fig. 4D – F)**. On the other hand – as illustrated in cluster-18, the F-F' loop may be oriented away from C-terminal loop resulting in a wider entrance (5.3 Å wider) for the OBS (termed as the 'open' conformation) **(Fig. 4F)**. To rationalize observed differences in F-F' loop conformation between the two CYP3A isoforms, we performed sequence alignment to identify key residue differences. Interestingly, Asp214 in CYP3A4 was found to be substituted to a more flexible Gly214 in CYP3A5 **(Supplementary Fig. 3)**. Apo and

Molecular Pharmacology Fast Forward. Published on July 1, 2021 as DOI: 10.1124/molpharm.121.000256
This article has not been copyedited and formatted. The final version may differ from this version.

holo crystal structures of CYP3A4 suggest that Asp214 plays an important role in stabilizing the 'closed' conformation of the F-F' loop by forming hydrogen bonds with Gly481 in the C-terminal loop **(Fig. 4A and B)**. While a complementary G479Q substitution is evident in the C-terminal loop of CYP3A5 **(Supplementary Fig. 3)**, apo and holo crystal structures reveal that Gln479 does not form any hydrogen bonds with residues on the opposing F-F' loop **(Fig. 4D and E)**. To further ascertain the impact of hydrogen bonding between F-F' and C-terminal loop in CYP3A5 on F-F' loop conformations and its ramifications in modulating the channel entrance, we computed the minimum distances between the backbone atoms of Gly214 from Gln479 side chain polar atoms and Gly480 (structurally equivalent to Gly481 in CYP3A4) backbone atoms (see **Supplementary Table 3** for more details) using apo-CYP3A5$_{WT}$ MD trajectories. Using a distance cut-off of 3.5 Å, we determined that Gly214 interacts with Gln479 and Gly480 in only 2.4% **(Fig. 5A)** and 6.5% **(Fig. 5B)** of the frames respectively. A comparative interaction analysis in apo-CYP3A5$_{MUT}$ MD trajectories revealed that while G214D form negligible interactions (0.3%) with Q479G **(Fig. 5C)**, G214D interestingly exhibited a substantially higher interaction frequency (23.3%) **(Fig. 5D)** with Gly480. Moreover, the interaction between G214D and Gly480 is very dynamic (**Supplementary Fig. 4**). Taken together, our findings suggest that the D214G substitution in CYP3A5 renders its F-F' loop more flexible than CYP3A4. Consequently, the CYP3A5 F-F' loop could move dynamically closer to the C-terminal loop in cluster-13 in one instance and further away from the C-terminal loop in cluster-18 in another instance **(Fig. 4F)**. When framed in the context of our *in vitro* findings, we posited that the dynamic flexibility of the F-F' loop in cluster-18 could have preserved substrate accessibility to

Molecular Pharmacology Fast Forward. Published on July 1, 2021 as DOI: 10.1124/molpharm.121.000256
This article has not been copyedited and formatted. The final version may differ from this version.

the OBS, explaining the lack of MBI despite covalent adduction by BBR epoxides at Ser239. Conversely, BBR adducts at Ser206 were found to be oriented further away from the F-F' loop and entrance to the OBS **(Supplementary Fig. 5)**, hence we are inclined to believe that covalent adduction at Ser206 is likely to be less pertinent to mechanistically explain the lack of MBI in CYP3A5.

Mixed-type Inhibition of CYP3A4 and CYP3A5 by BBR. Our earlier MBI screening assays **(Fig. 2)** also hinted that BBR could directly inhibit CYP3A4 and CYP3A5. Consequently, we proceeded to probe their mixed-type inhibitions to better characterize the nature of interaction between BBR and both CYP3A isoforms. Our findings demonstrated that BBR reversibly inhibited CYP3A4-mediated testosterone 6β-hydroxylation, midazolam 1'-hydroxylation and rivaroxaban hydroxylation with IC_{50} values (expressed as mean ± S.D) of 9.11 ± 1.1 μM, 21.47 ± 1.1 μM and 42.35 ± 6.34 μM respectively **(Fig. 6A – C)**. Similarly, when CYP3A5 was incubated with BBR, a characteristic sigmoidal dose-dependent decrease in testosterone 6β-hydroxylation and midazolam 1'-hydroxylation activities was evident with IC_{50} values (expressed as mean ± S.D) of 11.76 ± 2.0 M and 43.68 ± 2.31 μM respectively **(Fig. 6D and E)**. Intriguingly, this trend was not recapitulated in incubation mixtures comprising CYP3A5 and rivaroxaban. Rather, CYP3A5-mediated rivaroxaban hydroxylation was enhanced in a concentration-dependent manner by BBR **(Fig. 6F)**. Notably, this effect peaked at 10 μM, beyond which a decline in enzyme activity was observed instead. This apparent activation of CYP3A5 metabolism was only present with rivaroxaban and absent when the FDA-recommended prototypical probe substrates (i.e. testosterone and midazolam) were utilized **(Fig. 7A)**.

Molecular Pharmacology Fast Forward. Published on July 1, 2021 as DOI: 10.1124/molpharm.121.000256
This article has not been copyedited and formatted. The final version may differ from this version.

Heterotropic Activation of CYP3A5-mediated Rivaroxaban Hydroxylation by BBR. To further expound on the observed atypical kinetic phenomenon, we characterized its kinetics to quantitatively evaluate the impact of BBR on rivaroxaban affinity (K_m) and CYP3A5 rivaroxaban hydroxylation activity (V_{max}). Fitting the data to the Michaelis-Menten model demonstrated that apparent V_{max} was augmented while K_m (expressed as mean ± S.D) was reduced from 34.51 ± 12.67 μM to 23.91 ± 4.60 μM **(Fig. 7B)**. This yielded an estimated ~5.69-fold increase in apparent V_{max}/K_m ratio at the highest concentration of BBR (10 μM) and hints that the apparent intrinsic clearance of rivaroxaban by CYP3A5 increases in the presence of BBR **(Table 2)**. Taken together, our findings further substantiated heteroactivation of CYP3A5-mediated rivaroxaban hydroxylation by BBR.

Refinements in the heteroactivation kinetics were made using the two-site model proposed by Korzekwa *et al* (Korzekwa *et al.*, 1998) which produced good fits (R^2 = 0.99) **(Table 3)**. The K_m (expressed as mean ± S.D) of CYP3A5-mediated rivaroxaban hydroxylation in the absence of BBR was determined to be 36.72 ± 19.15 μM using the two-site model which is comparable to the value derived from the Michaelis-Menten model (34.51 ± 12.67 μM). Interaction factors α and β were determined to be 0.44 and 5.88 respectively **(Table 3)**. Since $\alpha < 1$ and $\beta > 1$, our results suggest that BBR activates the metabolism of rivaroxaban via a decrease in K_m and an increase in V_{max}. At this outset, this complex kinetic relationship is also observable from the three-dimensional surface plot **(Fig. 8)**. Finally, the K_B was determined to be 14.55 μM **(Table 3)**.

Effect of CYP3A Inhibitor on Heteroactivation. Activation of CYP3A5-mediated rivaroxaban hydroxylation by BBR was suppressed in the presence of 0.1 μM

Molecular Pharmacology Fast Forward. Published on July 1, 2021 as DOI: 10.1124/molpharm.121.000256
This article has not been copyedited and formatted. The final version may differ from this version.

ketoconazole **(Fig. 7C)**. However, the concentration-dependent enhancement of CYP3A5 metabolism was still apparent and similarly peaked at 10 μM of BBR. In contrast, co-incubation with 1 μM ketoconazole (~10× K_i) completely abolished heteroactivation elicited by BBR.

Effect of Pre-Incubation on Heteroactivation. To delineate whether heteroactivation is incited by parent BBR or its metabolites, the effects of pre-incubation was investigated. Our results reveal that enhancement of CYP3A5-mediated rivaroxaban hydroxylation decreased moderately with increasing pre-incubation time **(Fig. 7D)**.

Non-Covalent Docking of BBR and Rivaroxaban in CYP3A4 and CYP3A5. Our *in silico* structural analyses revealed that volumes of the OBS did not vary considerably between CYP3A4 (720.6 – 1360.0 $Å^3$) and CYP3A5 (889.6 – 1376.0 $Å^3$) **(Table 4 and 5)**. Additionally, non-covalent docking models revealed that in both docking schemes, the first ligand docked to the PBP (i.e. BBR in scheme 1 and rivaroxaban in scheme 2) in the absence of the second ligand in the DPB produced more favorable docking scores in CYP3A4 (average docking scores of -5.4 and -6.4 in scheme 1 and 2, respectively) as compared to that in CYP3A5 (average docking scores of -4.5 and -5.2 in scheme 1 and 2, respectively), thereby implying a higher binding affinity of the first ligand bound to CYP3A4 **(Table 4 and 5)**. On the contrary, after the PBP is occupied with the first docked ligand, the second ligand docked to the DBP (i.e. rivaroxaban in scheme 1 and BBR in scheme 2) exhibited an opposing trend in that CYP3A5 yielded more favorable binding scores (average docking scores of -7.7 and -6.3 in scheme 1 and 2, respectively) than CYP3A4 (average docking scores of -6.9 and -4.7 in scheme 1 and 2, respectively). This suggested a

Molecular Pharmacology Fast Forward. Published on July 1, 2021 as DOI: 10.1124/molpharm.121.000256
This article has not been copyedited and formatted. The final version may differ from this version.

greater likelihood for CYP3A5 to accommodate the second docked ligand in the presence of the first docked ligand. Concordant with these findings, we also observed smaller SASA values and ligand exposure from the second ligand docked to CYP3A5 (ligand exposure of 1.7 – 5.4% and 0.9 – 12.7% in scheme 1 and 2, respectively) than to CYP3A4 (ligand exposure of 8.0 – 26.7% and 8.8 – 27.0% in scheme 1 and 2, respectively) in all but one case **(Table 4 and 5)**.

Molecular Pharmacology Fast Forward. Published on July 1, 2021 as DOI: 10.1124/molpharm.121.000256
This article has not been copyedited and formatted. The final version may differ from this version.

DISCUSSION

In this study, we delineated the unique dichotomous interactions of BBR with CYP3A4 and CYP3A5 and characterized the kinetics and structural determinants underpinning their differing inactivation or activation profiles for the first time. As the CYP3A isoforms share ~85% sequence homology, we postulated that the observed differences in their interactions with BBR may be ascribed to the subtle yet important nuances in their active sites architecture which consequently facilitate differential irreversible or reversible interactions.

Using three structurally-distinct probe substrates of CYP3A, we confirmed the presence and absence of MBI by BBR against CYP3A4 and CYP3A5 respectively. Although it has been previously demonstrated experimentally that the reactive electrophilic epoxide metabolites of BBR was primarily generated by the CYP3A subfamily (Wang *et al.*, 2016), due to the low turnover rate of BBR by CYP3A5, it is plausible that the lack of observed MBI elicited by CYP3A5 in our assays could stem from its low intrinsic clearance which could also reduce the likelihood of generating the epoxide metabolite implicated in its MBI. To account for this, we have included a high concentration of BBR (25 μM) in our MBI screening experiments and allowed sufficient time for CYP3A5-mediated metabolism/bioactivation of BBR by pre-incubating BBR with CYP3A5 for up to 30 min before the subsequent introduction of the probe substrate. In spite of these, our findings consistently demonstrated a lack of MBI in CYP3A5 in all three CYP3A probe substrates utilized. As such, we posited that slight alterations in active site architecture of CYP3A4 and CYP3A5 could be responsible instead for its diverging MBI susceptibilities despite the bioactivation of BBR to its epoxides in both isoforms. Sequence alignments further revealed that

Molecular Pharmacology Fast Forward. Published on July 1, 2021 as DOI: 10.1124/molpharm.121.000256
This article has not been copyedited and formatted. The final version may differ from this version.

these two reactive cysteines that we previously identified in CYP3A4 are substituted to Trp58 and Ser239 in CYP3A5. Consequently, we initially proposed that discrepancies in the observed MBI susceptibilities between the two CYP3A isoforms may be attributed to the different nucleophilicities of the side chains in relation to their ability to sequester reactive metabolites generated via bioactivation. However, covalent docking models have since suggested that both Cys239 in CYP3A4 and Ser239 in CYP3A5 bear similar propensities to form adducts with BBR epoxide metabolites. While unexpected, it has been previously reported that covalent modification of the enzymatic active site need not always precipitate in a loss of enzyme activity (Barr *et al.*, 2020). At this outset, we are inclined to believe that there may be a more nuanced explanation underscoring the different MBI susceptibilities in both CYP3A isoforms. In that regard, additional structural insights gleaned from our docking models have proposed that BBR-Cys239 adducts in CYP3A4 stabilized a ‘closed’ conformation of the F-F’ loop which could restrict the approach of an incoming substrate into the OBS and result in enzyme inactivation. In contrast, MD simulations and docking models in CYP3A5 revealed that its F-F’ loop possesses a greater degree of structural flexibility which allowed for the subsequent stabilization of both a ‘closed’ and ‘open’ F-F’ loop conformation by BBR-Ser239 adducts. This is further substantiated by our apo-CYP3A5$_{MUT}$ MD trajectories which proposed that its structural flexibility results from D214G substitution in F-F’ loop of CYP3A5. As the F-F’ loop is oriented directly above the OBS and play an instrumental role in substrate-enzyme binding by functioning as a gating mechanism involved in substrate access and egress, its resulting conformation is anticipated to have important implications to substrate binding. Consequently, we postulated that the greater inherent flexibility

Molecular Pharmacology Fast Forward. Published on July 1, 2021 as DOI: 10.1124/molpharm.121.000256
This article has not been copyedited and formatted. The final version may differ from this version.

coupled with the maintenance of an 'open' F-F' loop conformation may have preserved substrate accessibility to the OBS and translated to a lack of MBI elicited by BBR in CYP3A5. However, it should be noted that our assertions here were based on covalent docking results of BBR epoxide metabolites to centroid frames extracted from MD simulations of CYP3A5 due to the inaccessibility of Ser239 in the two published crystal structures. Nonetheless, such an observation elegantly illustrates how the ensemble-based approach that we adopted for docking analysis could circumvent limitations associated with the lack of reported CYP3A5 crystal structures.

While interrogating the MBI susceptibilities of CYP3A4 and CYP3A5 by BBR, we observed a reduction in residual enzyme activity with increasing BBR concentrations in the absence of pre-incubation, implying possible reversible inhibition by BBR. Our experiments subsequently confirmed mixed-type inhibition of CYP3A4 with all three probe substrates utilized. Atypically, while we demonstrated that mixed-type inhibition of CYP3A5 could be recapitulated with testosterone and midazolam, there was an apparent enhancement of CYP3A5 activity when rivaroxaban was utilized as the probe substrate in the presence of BBR, hinting at a possible heterotropic activation of CYP3A5-mediated rivaroxaban hydroxylation by BBR. These serendipitous findings prompted us to characterize the observed heteroactivation using a more representative kinetic model that could simultaneously account for the kinetics of both the probe substrate and activator. Korzekwa *et al*. previously described a two-site model which was harnessed to fit heteroactivation of CYP3A-mediated metabolism of midazolam by erlotinib (Korzekwa *et al.*, 1998; Dong *et al.*, 2011). Here, we demonstrated that the two-site model could also provide a good fit

Molecular Pharmacology Fast Forward. Published on July 1, 2021 as DOI: 10.1124/molpharm.121.000256
This article has not been copyedited and formatted. The final version may differ from this version.

for our data (R^2 = 0.99). Interaction factors of α (0.44) and β (5.88) were in accordance with the criteria for activation (i.e. α < 1 and/or β > 1). Co-incubation with ketoconazole suppressed the enhancement of CYP3A5-mediated rivaroxaban hydroxylation in a concentration-dependent manner, further lending support to the notion that heteroactivation by BBR occurred within the active site (Houston and Galetin, 2005). Finally, considering that the amount of BBR decreased moderately with increasing pre-incubation time due to its metabolism by CYP3A5 and increasing pre-incubation time resulted in a reduction in activation of CYP3A5-mediated rivaroxaban hydroxylation to a similar extent, heteroactivation of CYP3A5 by BBR is possibly elicited by parent BBR and not its metabolites.

Current understanding on the structural and molecular determinants of heterotropic activation is tenuous but X-ray crystallographic evidence points towards the existence of a large active site with remarkable plasticity that can simultaneously accommodate two or more substrate molecules within different binding pockets. While both CYP3A4 and CYP3A5 are known to have considerably large active sites, a recently study reported that the active site cavity volume for CYP3A5 (1866 Å) was considerably larger than that in CYP3A4 (1386 Å) (Hsu *et al.*, 2018) which may explain the disparity in heteroactivation susceptibilities between the two CYP3A isoforms. However, the active site of CYP3A4 has also been previously found to be large enough to bind two or more bulky molecules (i.e. ketoconazole) (Sevrioukova and Poulos, 2013). Consequently, rather than differences in cavity size, it is plausible that active site architectural differences could instead favor different binding conformations for BBR and rivaroxaban such that the two may only coexist in CYP3A5 but not in CYP3A4 due to spatial and steric restrictions. In alignment with

Molecular Pharmacology Fast Forward. Published on July 1, 2021 as DOI: 10.1124/molpharm.121.000256
This article has not been copyedited and formatted. The final version may differ from this version.

this postulation, our *in silico* analyses have shown that when the PBP is occupied by the first docked ligand (i.e. rivaroxaban or BBR), there is a greater binding affinity for the second docked ligand in the DBP of CYP3A5 than in CYP3A4 – regardless of the order of docking. This observation is substantiated by the lower SASA and ligand exposure values for the second ligand docked to the DBP in CYP3A5 than in CYP3A4. Thereby, implying that in comparison to CYP3A4, the OBS of CYP3A5 can more favorably accommodate both BBR and rivaroxaban in concert which could potentially explain our *in vitro* observations pertaining to the heteroactivation of rivaroxaban metabolism by BBR in CYP3A5 but not in CYP3A4. At its core, modelling atypical kinetics is most rigorous when supported by mechanistic insights describing such enzyme-substrate interactions at a molecular level. As such, we hypothesize that elucidating the precise binding poses of BBR and rivaroxaban in CYP3A5 is key to understanding the mechanism of heteroactivation of rivaroxaban metabolism by BBR. While unelucidated, a plausible mechanism could arise from initial binding of BBR to the effector binding pocket near the heme moiety in CYP3A5 which in turns elicits a conformational change in the substrate binding pocket that increases binding affinity towards rivaroxaban. Finally, it should be noted that while the *in silico* assays described in this study do not yield direct experimental evidence, they provide plausible and key mechanistic insights on the molecular determinants underpinning their diverging reversible and irreversible interaction profiles. Consequently, additional work involving site-directed mutagenesis and/or MS-based proteomics need to be performed to validate our conjectures.

In conclusion, our findings demonstrated that BBR exhibits differential interactions with CYP3A4 and CYP3A5. Specifically, BBR irreversibly inactivates CYP3A4 via

Molecular Pharmacology Fast Forward. Published on July 1, 2021 as DOI: 10.1124/molpharm.121.000256
This article has not been copyedited and formatted. The final version may differ from this version.

MBI whereas BBR reversibly activates CYP3A5-mediated rivaroxaban hydroxylation through heterotropic cooperative interactions. Disparities in the susceptibility towards MBI was suggested to be attributed to the effects of covalent adducts on the F-F' loop. Our findings here illuminate the atypical dichotomous inactivation and activation kinetics between BBR and the two highly homologous CYP3A isoforms and pave the way for future investigations into their clinical implications. Finally, these results reinforce the importance of discerning between the kinetic behavior of CYP3A4 and CYP3A5 due to their propensities for diverging interaction profiles with a common substrate.

Molecular Pharmacology Fast Forward. Published on July 1, 2021 as DOI: 10.1124/molpharm.121.000256
This article has not been copyedited and formatted. The final version may differ from this version.

AUTHORSHIP CONTRIBUTIONS

Participated in research design:	Tang, Verma, Fan, Chan
Conducted experiments:	Tang, Verma, Yong
Contributed new reagents or analytical tools:	Lin, Fan
Performed data analysis:	Tang, Verma, Yong, Li, Wang
Wrote or contributed to the writing of the manuscript:	Tang, Verma, Li, Wang, Fan, Chan

REFERENCES

Abraham MJ, Murtola T, Schulz R, Páll S, Smith JC, Hess B, and Lindah E (2015) GROMACS: High performance molecular simulations through multi-level parallelism from laptops to supercomputers. *SoftwareX* **1**–**2**:19–25.

Barr JT, Wang Z, Min X, Wienkers HJ, Rock BM, Rock DA, and Wienkers LC (2020) Mechanistic Studies of Cytochrome P450 3A4 Time-Dependent Inhibition Using Two Cysteine-Targeting Electrophiles. *Drug Metab Dispos* **48**:508–514.

Best RB, Zhu X, Shim J, Lopes PEM, Mittal J, Feig M, and MacKerell AD (2012) Optimization of the additive CHARMM all-atom protein force field targeting improved sampling of the backbone φ, ψ and side-chain χ1 and χ2 Dihedral Angles. *J Chem Theory Comput* **8**:3257–3273.

Bjornsson TD, Callaghan JT, Einolf HJ, Fischer V, Gan L, Grimm S, Kao J, King SP, Miwa G, Ni L, Kumar G, McLeod J, Obach RS, Roberts S, Roe A, Shah A, Snikeris F, Sullivan JT, Tweedie D, Vega JM, Walsh J, and Wrighton SA (2003) The conduct of in vitro and in vivo drug-drug interaction studies: A Pharmaceutical Research and Manufacturers of America (PhRMA) perspective. *Drug Metab Dispos* **31**:815–832.

Chan ECY, New LS, Chua TB, Yap CW, Ho HK, and Nelson SD (2012) Interaction of lapatinib with cytochrome P450 3A5. *Drug Metab Dispos* **40**:1414–1422.

Darden T, York D, and Pedersen L (1993) Particle mesh Ewald: An N·log(N) method for Ewald sums in large systems. *J Chem Phys* **98**:10089–10092.

Dong PP, Fang ZZ, Zhang YY, Ge GB, Mao YX, Zhu LL, Qu YQ, Li W, Wang LM, Liu CX, and Yang L (2011) Substrate-dependent modulation of the catalytic activity of CYP3A by erlotinib. *Acta Pharmacol Sin* **32**:399–407, Nature Publishing Group.

Friesner RA, Banks JL, Murphy RB, Halgren TA, Klicic JJ, Mainz DT, Repasky MP, Knoll EH, Shelley M, Perry JK, Shaw DE, Francis P, and Shenkin PS (2004) Glide: A New Approach for Rapid, Accurate Docking and Scoring. 1. Method and Assessment of Docking Accuracy. *ACS Publ* **47**:1739–1749.

Greenblatt DJ, Zhao Y, Venkatakrishnan K, Duan SX, Harmatz JS, Parent SJ, Court MH, and Von Moltke LL (2011) Mechanism of cytochrome P450-3A inhibition by ketoconazole. *J Pharm Pharmacol* **63**:214–221.

Guo X, Li W, Li Q, Chen Y, Zhao G, Peng Y, and Zheng J (2019) Tofacitinib Is a Mechanism-Based Inactivator of Cytochrome P450 3A4. *Chem Res Toxicol* **32**:1791–1800.

Hong Y, Chia YMF, Yeo RH, Venkatesan G, Koh SK, Chai CLL, Zhou L, Kojodjojo P, and Chan ECY (2016) Inactivation of human cytochrome P450 3A4 and 3A5 by dronedarone and n-desbutyl dronedarone. *Mol Pharmacol* **89**:1–13, American Society for Pharmacology and Experimental Therapy.

Hoover WG (1985) Canonical dynamics: Equilibrium phase-space distributions. *Phys Rev A* **31**:1695–1697.

Houston JB, and Galetin A (2005) Modelling atypical CYP3A4 kinetics: Principles and pragmatism. *Arch Biochem Biophys* **433**:351–360.

Hsu MH, and Johnson EF (2019) Active-site differences between substrate-free and ritonavirbound cytochrome P450 (CYP) 3A5 reveal plasticity differences between CYP3A5 and CYP3A4. *J Biol Chem* **294**:8015–8022.

Hsu MH, Savas U, and Johnson EF (2018) The X-ray crystal structure of the human mono-oxygenase cytochrome P450 3A5-ritonavir complex reveals active site differences between P450s 3A4 and 3A5. *Mol Pharmacol* **93**:14–24.

Jo S, Kim T, Iyer VG, and Im W (2008) CHARMM-GUI: A web-based graphical user interface for CHARMM. *J Comput Chem* **29**:1859–1865.

Jorgensen WL, Chandrasekhar J, Madura JD, Impey RW, and Klein ML (1983) Comparison of simple potential functions for simulating liquid water. *J Chem Phys* **79**:926–935.

Kamdem LK, Streit F, Zanger UM, Brockmöller J, Oellerich M, Armstrong VW, and Wojnowski L (2005) Contribution of CYP3A5 to the in vitro hepatic clearance of tacrolimus. *Clin Chem* **51**:1374–1381.

Kamel A, and Harriman S (2013) Inhibition of cytochrome P450 enzymes and biochemical aspects of mechanism-based inactivation (MBI). *Drug Discov Today Technol* **10**:e177–e189, Elsevier Ltd.

Kim S, Chen J, Cheng T, Gindulyte A, and He J (2018) PubChem 2019 update: improved access to chemical data. *Nucleic Acids Res* **47**:1102–1109.

Kitagawara Y, Ohe T, Tachibana K, Takahashi K, Nakamura S, and Mashino T (2015) Novel bioactivation pathway of benzbromarone mediated by cytochrome P450. *Drug Metab Dispos* **43**:1303–1306.

Korzekwa KR, Krishnamachary N, Shou M, Ogai A, Parise RA, Rettie AE, Gonzalez FJ, and Tracy TS (1998) Evaluation of Atypical Cytochrome P450 Kinetics with Two-Substrate Models: Evidence That Multiple Substrates Can Simultaneously Bind to Cytochrome P450 Active Sites †. *Biochemistry* **37**:4137–4147.

Lamba JK, Lin YS, Schuetz EG, and Thummel KE (2002) Genetic contribution to variable human CYP3A-mediated metabolism. *Adv Drug Deliv Rev* **54**:1271–1294.

Lin YS, Dowling ALS, Quigley SD, Farin FM, Zhang J, Lamba J, Schuetz EG, and Thummel KE (2002) Co-regulation of CYP3A4 and CYP3A5 and contribution to hepatic and intestinal midazolam metabolism. *Mol Pharmacol* **62**:162–172.

Nosé S, and Klein ML (1983) Constant pressure molecular dynamics for molecular systems. *Mol Phys* **50**:1055–1076.

Okada Y, Murayama N, Yanagida C, Shimizu M, Guengerich FP, and Yamazaki H (2009) Drug interactions of thalidomide with midazolam and cyclosporine a: heterotropic cooperativity of human cytochrome P450 3A5. *Drug Metab Dispos* **37**:18–23.

Pearson JT, Wahlstrom JL, Dickmann LJ, Kumar S, Halpert JR, Wienkers LC, Foti RS, and Rock DA (2007) Differential time-dependent inactivation of P450 3A4 and P450 3A5 by raloxifene: A key role for C239 in quenching reactive intermediates. *Chem Res Toxicol* **20**:1778–1786.

Rose PW, Prlić A, Bi C, Bluhm WF, Christie CH, Dutta S, Green RK, Goodsell DS, Westbrook JD, Woo J, Young J, Zardecki C, Berman HM, Bourne PE, and Burley SK (2015) The RCSB Protein Data Bank: Views of structural biology for basic and applied research and education. *Nucleic Acids Res* **43**:D345–D356, Oxford University Press.

Sevrioukova IF, and Poulos TL (2010) Structure and mechanism of the complex between cytochrome P4503A4 and ritonavir. *Proc Natl Acad Sci U S A* **107**:18422–18427, National Academy of Sciences.

Sevrioukova IF, and Poulos TL (2013) Understanding the Mechanism of Cytochrome P450 3A4: Recent Advances and Remaining Problems. *Dalt Trans* **42**:3116–3126.

Sugiyama M, Fujita K, Murayama N, Akiyama Y, Yamazaki H, and Sasaki Y (2011) Sorafenib and sunitinib, two anticancer drugs, inhibit CYP3A4-mediated and activate CY3A5-mediated midazolam 1'-hydroxylation. *Drug Metab Dispos* **39**:757–762.

Tang LWT, Verma RK, Fan H, and Chan ECY (2021) Mechanism-Based Inactivation of Cytochrome P450 3A4 by Benzbromarone. *Mol Pharmacol* **99**:266–276, American Society for Pharmacology and Experimental Therapeutics.

Tracy TS (2006) Atypical cytochrome P450 kinetics: Implications for drug discovery. *Drugs R D* **7**:349–363.

Tseng E, Walsky RL, Luzietti RA, Harris JJ, Kosa RE, Goosen TC, Zientek MA, and Obach RS (2014) Relative contributions of cytochrome CYP3A4 versus CYP3A5 for CYP3A-cleared drugs assessed in vitro using a CYP3A4-selective inactivator (CYP3cide). *Drug Metab Dispos* **42**:1163–1173, American Society for Pharmacology and Experimental Therapy.

Wang H, Wang W, Gong B, Wang Z, Feng Y, Zhang W, Wang S, Peng Y, and Zheng J (2019) Glutathione conjugation and protein adduction derived from oxidative debromination of benzbromarone in mice. *Drug Metab Dispos* **47**:1281–1290.

Wang J-X, Zhang C, Fu L, Zhang D-G, Wang B-W, Zhang Z-H, Chen Y-H, Lu Y, Chen X, and Xu D-X (2017) Protective effect of rosiglitazone against acetaminophen-induced acute liver injury is associated with down-regulation of hepatic NADPH oxidases. *Toxicol Lett* **265**:38–46.

Wang J, Wang W, Kollman PA, and Case DA (2006) Automatic atom type and bond type perception in molecular mechanical calculations. *J Mol Graph Model* **25**:247–260.

Wang K, Wang H, Peng Y, and Zheng J (2016) Identification of epoxide-derived metabolite(s) of benzbromarone. *Drug Metab Dispos* **44**:607–615.

Wilkinson GR (1996) Cytochrome P4503A (CYP3A) metabolism: Prediction of in vivo activity in humans. *J Pharmacokinet Biopharm* **24**:475–490.

Wrighton SA, VandenBranden M, and Ring BJ (1996) The human drug metabolizing cytochromes P450. *J Pharmacokinet Biopharm* **24**:461–473.

Yano JK, Wester MR, Schoch GA, Griffin KJ, Stout CD, and Johnson EF (2004) The structure of human microsomal cytochrome P450 3A4 determined by X-ray crystallography to 2.05-Å resolution. *J Biol Chem* **279**:38091–38094, American Society for Biochemistry and Molecular Biology.

Zhu K, Borrelli KW, Greenwood JR, Day T, Abel R, Farid RS, and Harder E (2014) Docking covalent inhibitors: A parameter free approach to pose prediction and scoring. *J Chem Inf Model* **54**:1932–1940, American Chemical Society.

Molecular Pharmacology Fast Forward. Published on July 1, 2021 as DOI: 10.1124/molpharm.121.000256
This article has not been copyedited and formatted. The final version may differ from this version.

FOOTNOTES

This work is supported by the Agency for Science, Technology and Research (A*STAR) Industry Alignment Fund – Pre-Positioning (IAF-PP) Funding [Grant H18/01/a0/C14] provided to H.F and E.C.Y.C and the National University Heart Centre Singapore (NUHCS) Cardiovascular Research Institute (CVRI) - Core Fund [Grant NUHSRO/2019/082/Core] and SCEPTRE CG Seed Grant [Grant NMRC/CG/M008/2017] provided to E.C.Y.C. L.W.T.T is supported by the National University of Singapore (NUS) President's Graduate Fellowship (PGF).

The authors declare that they have no conflicts of interest with the contents of this article.

Molecular Pharmacology Fast Forward. Published on July 1, 2021 as DOI: 10.1124/molpharm.121.000256
This article has not been copyedited and formatted. The final version may differ from this version.

FIGURE LEGENDS

Fig. 1. Chemical structures of (A) BBR and its epoxide reactive metabolites (B) BBR-6,7-BF-Epoxide and (C) BBR-5,6-BF-Epoxide.

Fig. 2. Screening for the MBI of CYP3A4 and CYP3A5 by BBR using (A and D) testosterone, (B and E) midazolam and (C and F) rivaroxaban as probe substrate. No apparent time-dependent decrease in CYP3A5 activity elicited by BBR is observed. Each point in (A to F) represents the mean and S.D of triplicate experiments.

Fig. 3. CYP3A5 adducts at Ser239. Centroid frames from (A) cluster-13 and (B) cluster-18. BBR-6,7-BF-Epoxide and BBR-5,6-BF-Epoxide are shown in different shades.

Fig. 4. F-F' loop conformations of CYP3A4 and CYP3A5 in their apo-, holo-(ritonavir-bound) and BBR adduct forms. (A) 'Closed' F-F' loop conformation of apo CYP3A4 (PDB:1TQN). (B) 'Closed' F-F' loop conformation of ritonavir-bound CYP3A4 (PDB:3NXU). (C) 'Closed' F-F' loop conformation of BBR-adducted CYP3A4 (PDB:3NXU and 4I4G). (D) 'Closed' F-F' loop conformation of apo CYP3A5 (PDB:6MJM). (E) 'Closed' F-F' loop conformation of ritonavir-bound CYP3A5 (PDB:5VEU). (F) 'Open' (cluster-18) or 'closed' (cluster-13) F-F' loop conformation of BBR-adducted CYP3A5. The F-F' and C-terminal residues within 5 Å of each other are shown in sticks. Shade of the F-F' and C-terminal loops corresponds to the respective PDB/Cluster ID code.

Fig. 5. Plots showing distribution of minimum distances between the hydrogen-bond forming atoms G214 from (A) Q479 and (B) G480 in apo-CYP3A5$_{WT}$ and G214D

Molecular Pharmacology Fast Forward. Published on July 1, 2021 as DOI: 10.1124/molpharm.121.000256
This article has not been copyedited and formatted. The final version may differ from this version.

from (C) Q479G and (D) G480 in apo-CYP3A5$_{MUT}$. The hydrogen-bond interaction cutoff of 3.5 Å is illustrated with a vertical dashed black line.

Fig. 6. IC_{50} curves depicting mixed-type inhibition elicited by BBR against CYP3A4, using (A) testosterone, (B) midazolam and (C) rivaroxaban as the probe substrate, and against CYP3A5, using (D) testosterone and (E) midazolam as the probe substrate. Apparent enhancement of CYP3A5 enzymatic activity by BBR is seen when (F) rivaroxaban was adopted as the probe substrate. Each point in (A to F) represents the mean and S.D of triplicate experiments.

Fig. 7. Heterotropic activation of CYP3A5-mediated rivaroxaban hydroxylation activity by BBR. (A) Heterotropic activation of CYP3A5 by BBR exhibits probe-substrate specificity. (B) Kinetics of heteroactivation of CYP3A5 by BBR, fitted to the Michaelis-Menten model. (C) Concentration-dependent suppression of heterotropic activation of CYP3A5 by BBR in the presence of potent CYP3A inhibitor ketoconazole. (D) Decreased activation of CYP3A5 by BBR with an increase in its pre-incubation time. Each bar graph and point in (A to D) represents the mean and S.D of triplicate experiments.

Fig. 8. Three-dimensional surface plot representing the heteroactivation of CYP3A5-mediated rivaroxaban hydroxylation by BBR, fitted to the two-site model. Each point in the surface plot represents the mean of triplicate experiments.

Molecular Pharmacology Fast Forward. Published on July 1, 2021 as DOI: 10.1124/molpharm.121.000256
This article has not been copyedited and formatted. The final version may differ from this version.

Table 1. Top covalent docking scores for BBR epoxide metabolites in CYP3A4 and CYP3A5

Residue	PDB/ Cluster ID	Covalent Docking Score		Reference
		BBR-6,7-BF-Epoxide	**BBR-5,6-BF-Epoxide**	
Ser239 (CYP3A5)	Cluster-13	-4.4[#]	-2.7	
	Cluster-18	-3.3	-3.0[#]	
Cys239 (CYP3A4)	4I4G	-3.1	-3.5	Tang *et al,* 2021

[#]MD frame with the top covalent docking score

Molecular Pharmacology Fast Forward. Published on July 1, 2021 as DOI: 10.1124/molpharm.121.000256
This article has not been copyedited and formatted. The final version may differ from this version.

Table 2. Kinetic parameter estimates for CYP3A5-mediated rivaroxaban hydroxylation in the absence or presence of BBR obtained by fitting to the Michaelis-Menten model. K_m is presented as means ± S.D of triplicate experiments whereas the apparent V_{max}/K_m ratio is presented as mean (95% CI).

BBR (μM)	**K_m (μM)**	**Apparent V_{max}/K_m ratio**	**Fold change in apparent V_{max}/K_m ratio (versus vehicle)**
0 (vehicle)	34.51 ± 12.67	0.79 (0.51 - 1.23)	-
1	33.65 ± 9.85	1.23 (0.88 – 1.75)	1.55
3	28.28 ± 5.64	2.40 (1.86 – 3.09)	3.03
10	23.91 ± 4.60	4.50 (3.54 – 5.70)	5.69

Molecular Pharmacology Fast Forward. Published on July 1, 2021 as DOI: 10.1124/molpharm.121.000256
This article has not been copyedited and formatted. The final version may differ from this version.

Table 3. Kinetic parameter estimates for the heteroactivation of CYP3A5-mediated rivaroxaban hydroxylation by BBR obtained by fitting to the two-site model. Data are presented as means ± S.D of triplicate experiments.

K_m (μM)	K_B (μM)	α	β	R^2
36.72 ± 19.15	14.55 ± 12.08	0.44 ± 0.54	5.88 ± 3.02	0.99

Molecular Pharmacology Fast Forward. Published on July 1, 2021 as DOI: 10.1124/molpharm.121.000256
This article has not been copyedited and formatted. The final version may differ from this version.

Table 4. Summary of docking results for scheme 1 in which BBR was first docked in the PBP after which rivaroxaban was docked in the DBP in the presence of BBR in the PBP.

CYP	PDB/ Cluster ID	OBS Volume (Å^3)	PBP Ligand (BBR)		DBP Ligand (Rivaroxaban)		
			Distance (Å)[#]	Docking Score	Docking Score	SASA (Å^2)	Ligand Exposure (%)
CYP 3A4	5TE8^ (holo)	720.6	3.20	-6.1	-4.3	184.9	26.7
	6BCZ^ (holo)	843.1	3.52	-5.2	-7.1	159.1	23.2
	3TJS (holo)	1360.0	3.97	-5.1	-7.4	90.6	13.2
	4I4H (holo)	1158.3	4.44	-5.2	-8.7	54.5	8.0
CYP 3A5	5VEU (holo)	889.6	3.01	-5.0	-8.0	10.5	1.7
	Cluster-2 (apo)	1322.8	4.60	-4.9	-7.6	24.6	3.6
	Cluster-20 (apo)	1376.0	3.66	-3.7	-8.1	27.2	4.0
	Cluster-28 (holo)	1168.6	4.86	-4.3	-7.2	35.1	5.4

^Rivaroxaban bound in DBP is partially exposed to bulk water

[#]Distance between the hydroxyl oxygen atom in the 2,6-dibromophenol group in BBR and heme iron.

Molecular Pharmacology Fast Forward. Published on July 1, 2021 as DOI: 10.1124/molpharm.121.000256
This article has not been copyedited and formatted. The final version may differ from this version.

Table 5. Summary of docking results for scheme 2 in which rivaroxaban was first docked in the PBP after which BBR was docked in the DBP in the presence of rivaroxaban in the PBP.

CYP	PDB/ Cluster ID	OBS Volume (Å^3)	PBP Ligand (Rivaroxaban)		DBP Ligand (BBR)		
			Distance (Å)[#]	Docking Score	Docking Score	SASA (Å^2)	Ligand Exposure (%)
CYP 3A4	5TE8^ (holo)	720.6	3.52	-6.6	-3.4	112.4	20.9
	6BCZ^ (holo)	843.1	2.56	-5.5	-3.0	146.3	27.0
	3TJS (holo)	1360.0	3.54	-6.2	-5.2	82.0	14.8
	4I4H (holo)	1158.3	3.36	-7.3	-7.3	48.4	8.8
CYP 3A5	5VEU (holo)	889.6	2.63	-5.6	-7.6	5.0	0.9
	Cluster-2 (apo)	1322.8	2.96	-5.3	-6.4	19.7	3.6
	Cluster-20 (apo)	1376.0	4.09	-5.2	-4.9	68.0	12.7
	Cluster-28 (holo)	1168.6	3.27	-4.8	-6.3	34.3	6.3

^Rivaroxaban bound in DBP is partially exposed to bulk water

[#]Distance between the oxygen atom in the morpholinone moiety of rivaroxaban and heme iron

Figure 1

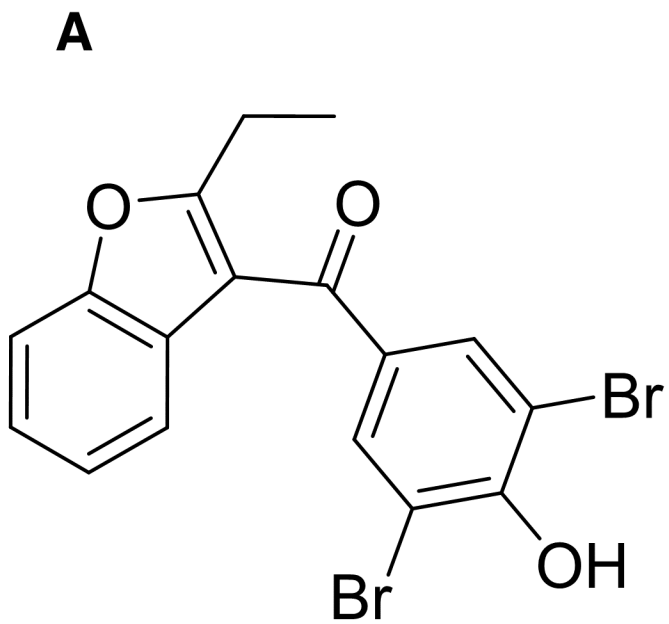

BBR

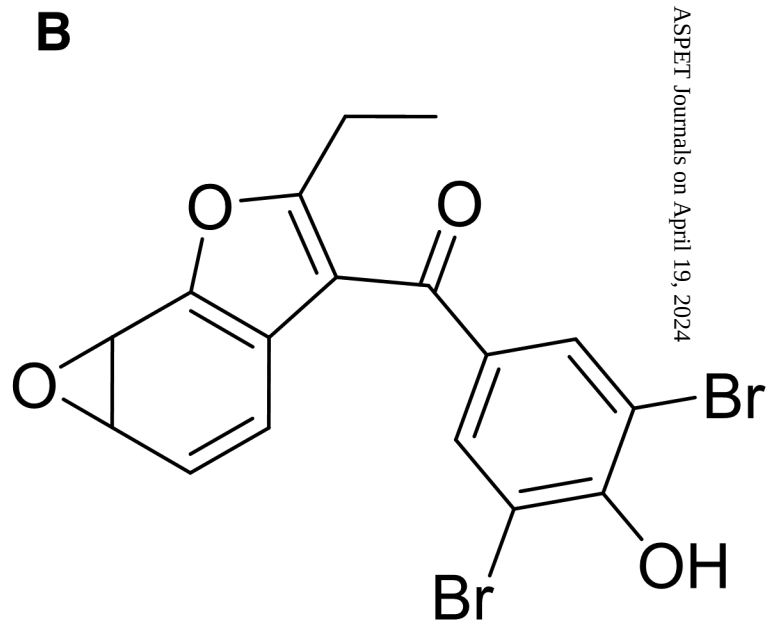

BBR-6,7-BF-Epoxide

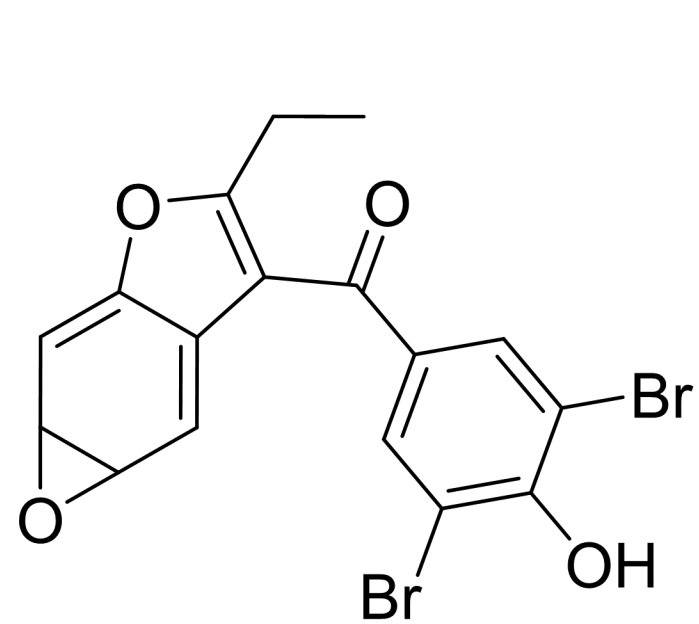

BBR-5,6-BF-Epoxide

Figure 2

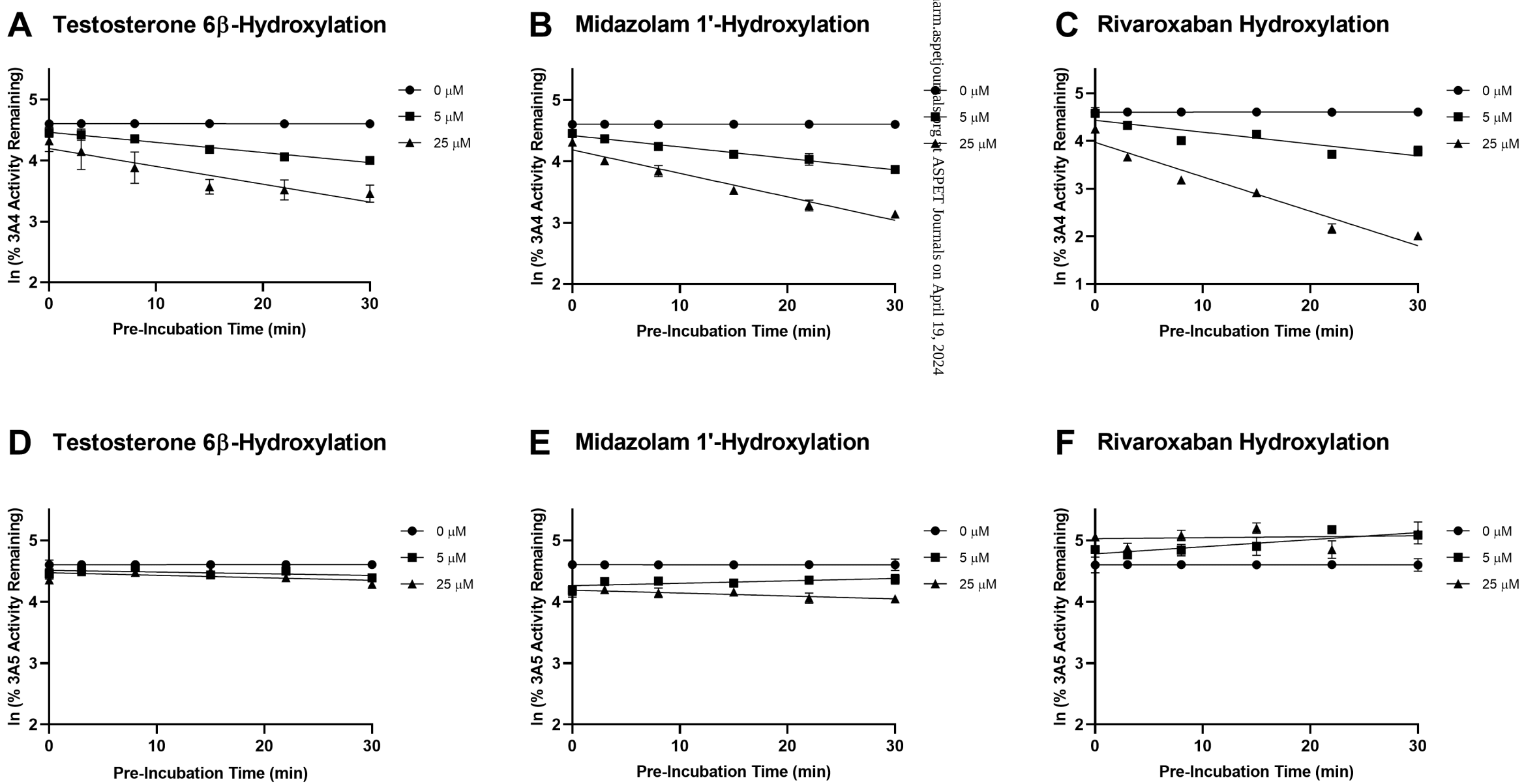

Figure 3

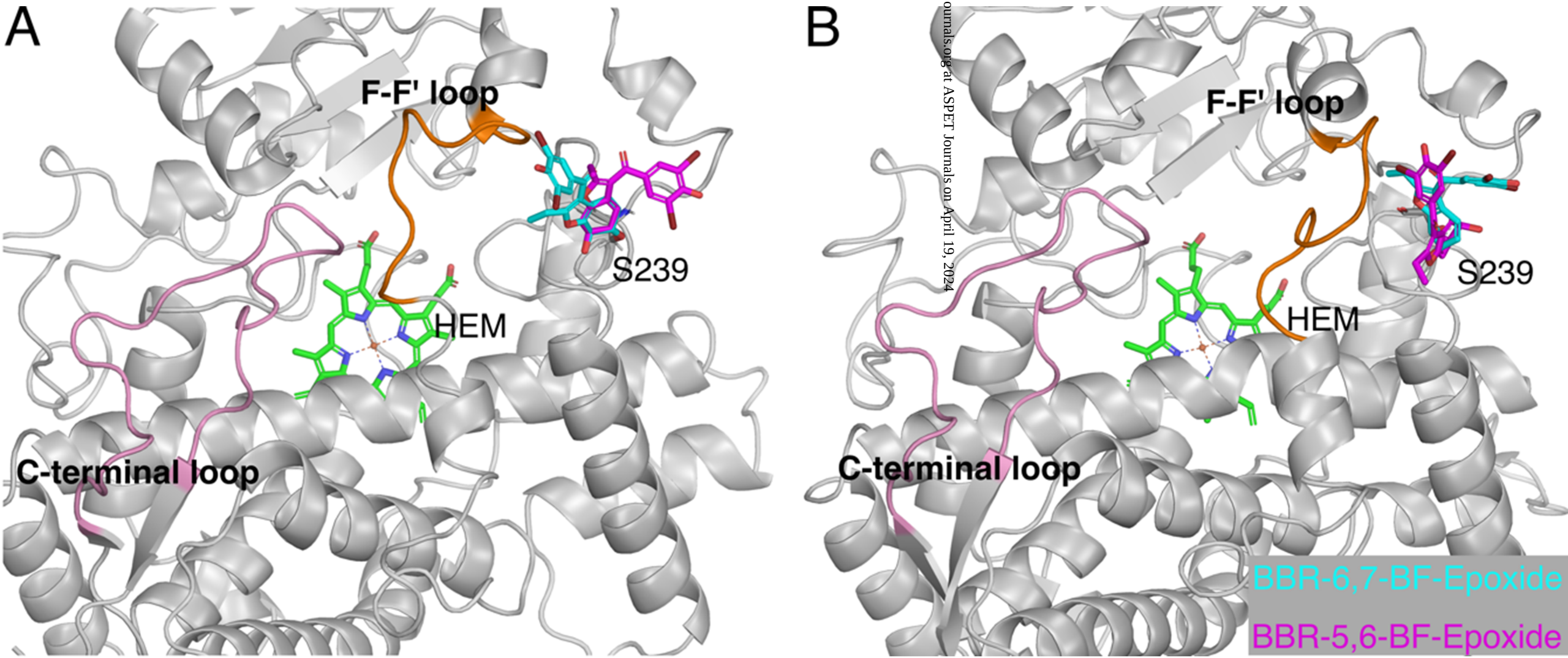

Figure 4

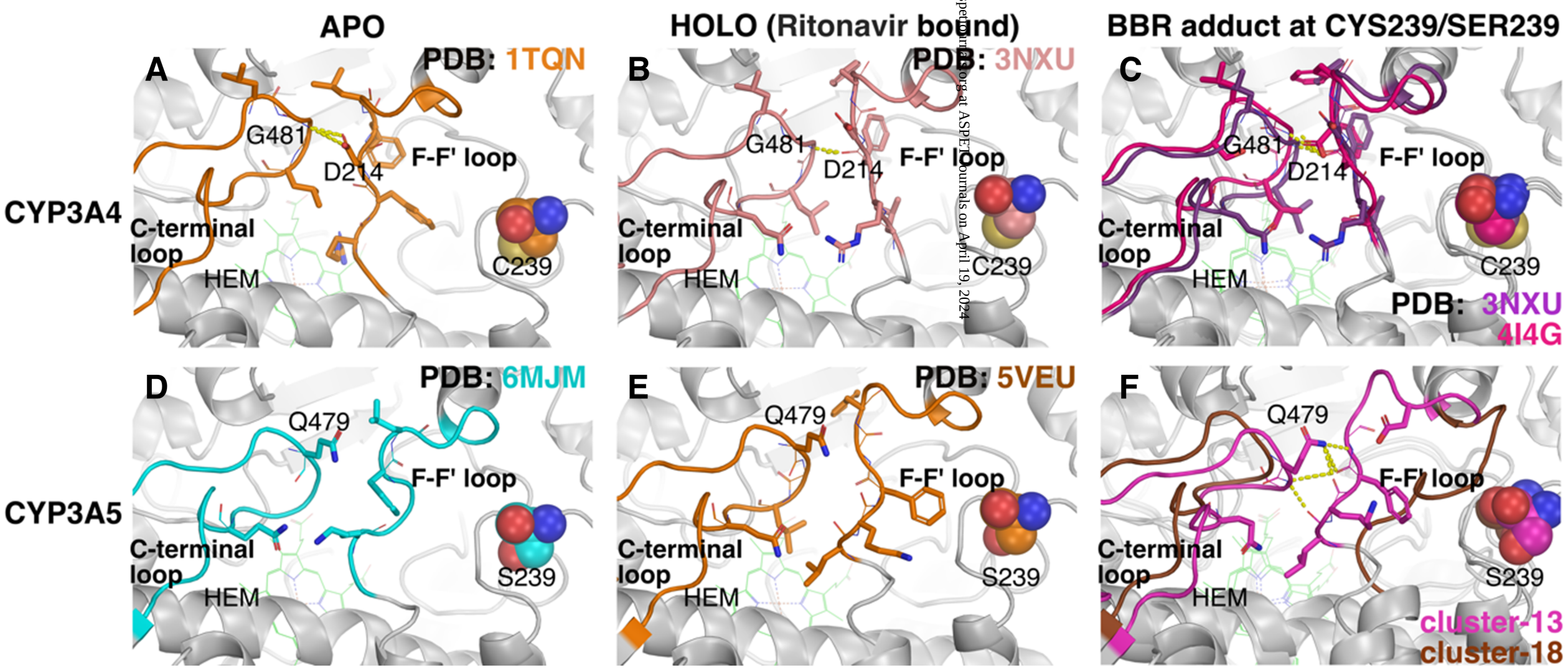

Figure 5

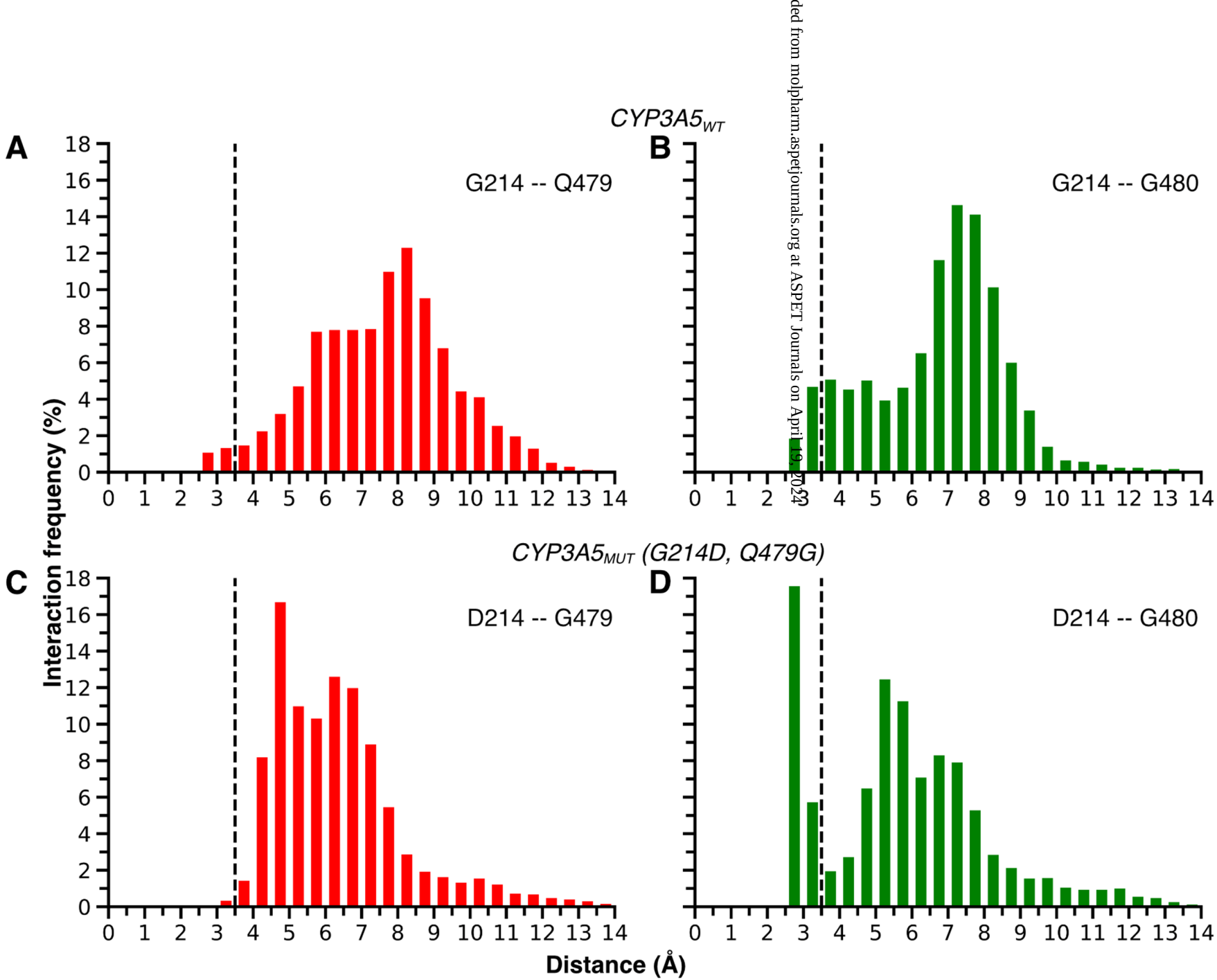

Figure 6

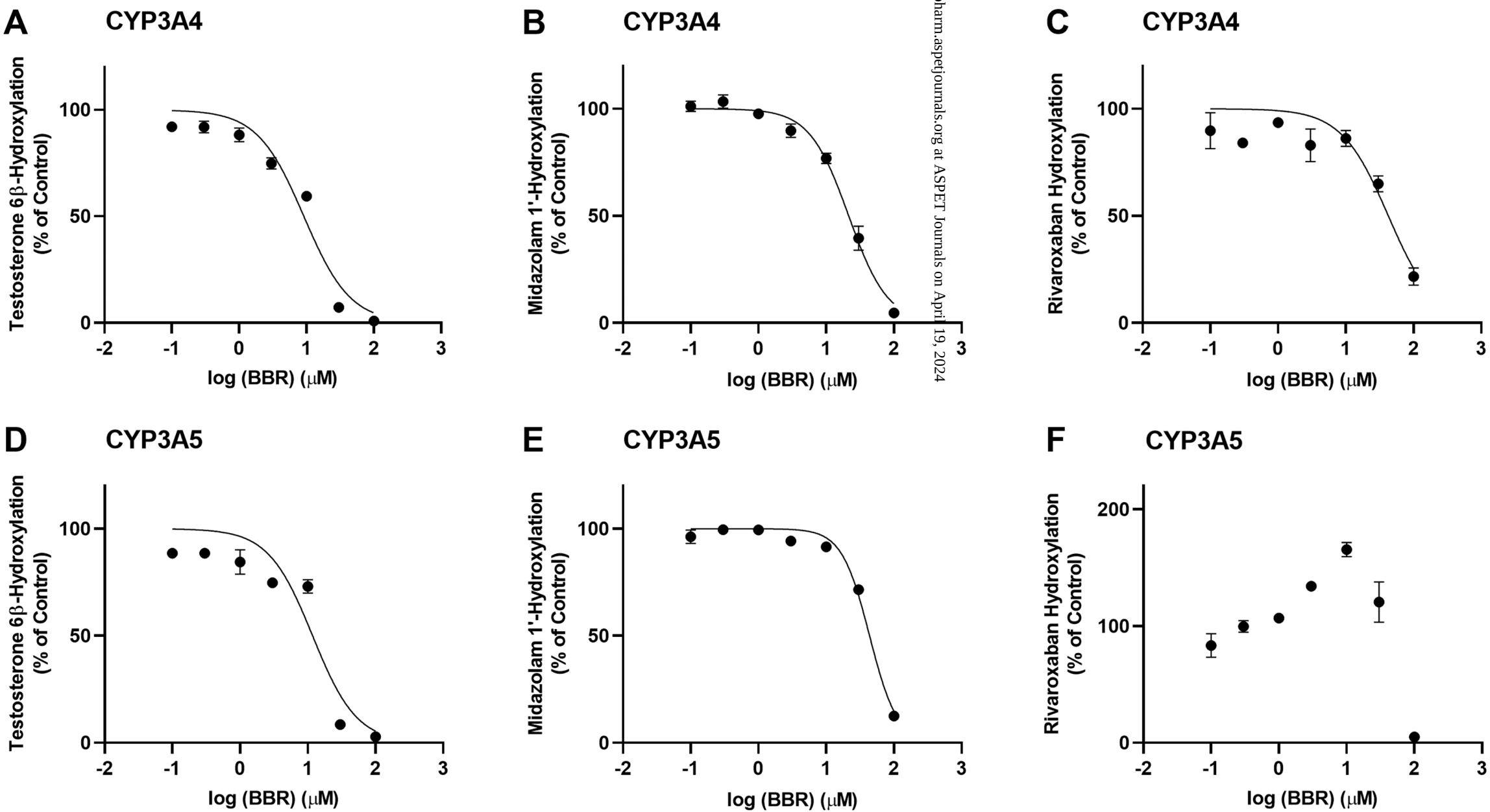

Figure 7

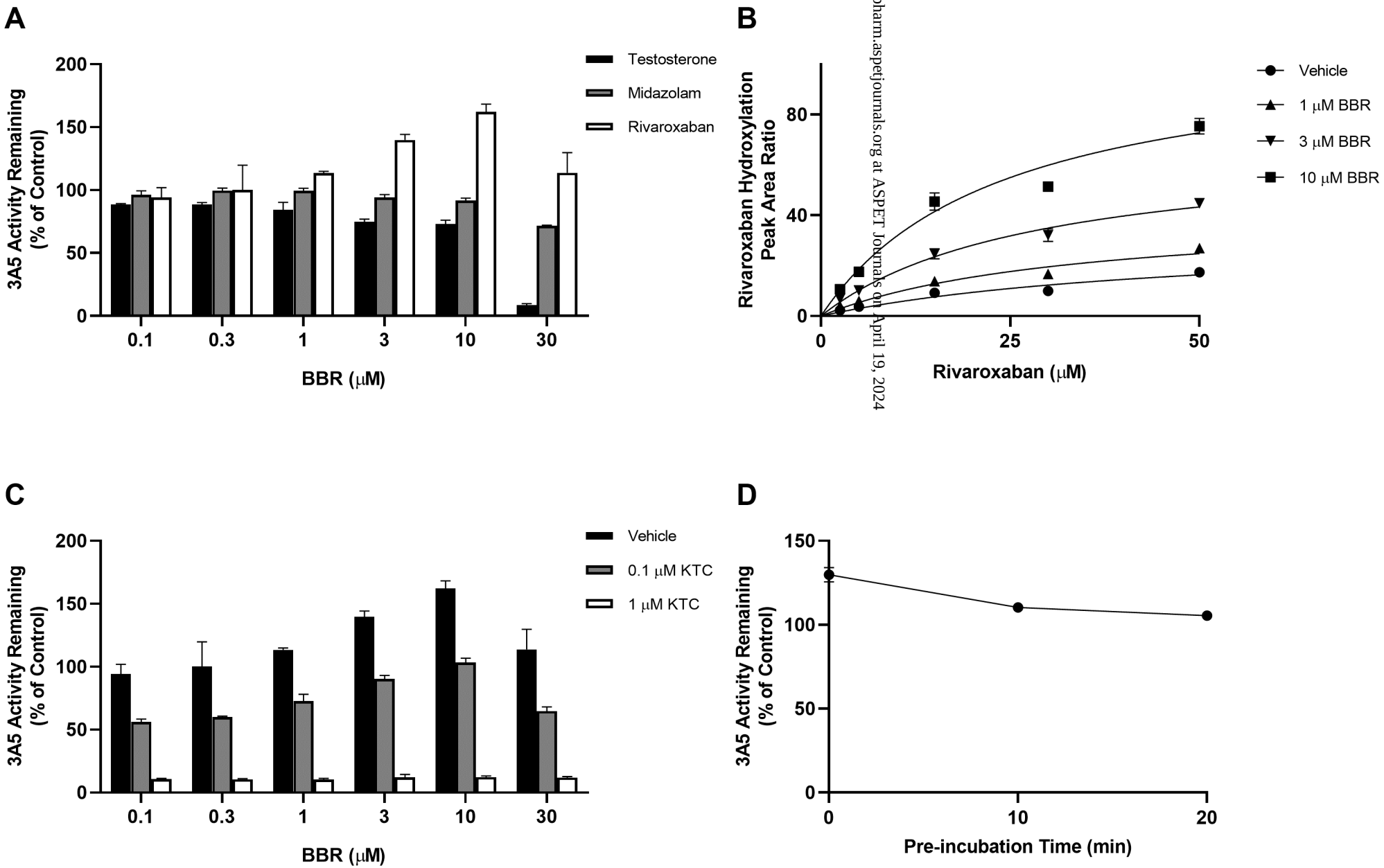

Figure 8